INTERNATIONAL JOURNAL OF
NUMERICAL ANALYSIS AND MODELING
Volume 20, Number 1, Pages 67–91

doi: 10.4208/ijnam2023-1004

A SPRING–BEAM SYSTEM WITH SIGNORINI'S CONDITION AND THE NORMAL COMPLIANCE CONDITION

JEONGHO AHN* AND NICHOLAS TATE

Abstract. This paper provides mathematical and numerical analyses for a dynamic frictionless contact problem in which both of Signorini's condition and the normal compliance condition are used. The contact problem is considered by employing two viscoelastic (Kelvin-Voigt type) objects: a linear Timoshenko beam and a nonlinear spring. In addition, a transmission condition is imposed on one end of the beam and the top of the spring so that they can touch and vibrate together. We prove the existence of solutions satisfying all the conditions. Time discretizations and finite element methods are utilized to propose the fully discrete numerical schemes. We select several groups of data to present and discuss numerical simulations.

Key words. Timoshenko beams, duffing equation, normal compliance, Signorini's condition, Galerkin's method, contraction mapping argument.

1. Introduction

Over the past half century, mathematical theories and numerical methods of contact mechanics have made remarkable progress. Reader may refer to the monographs [6, 7] to understand mathematical and numerical approaches to contact problems with various effects such as friction, wear, thermal effects, adhesion, or damage. In particular, one–dimensional dynamic contact problems for strings, rods, or beams with or without those side effects have been actively studied. See, e.g., [21, 23, 19, 15, 20, 16, 9, 17, 18]. If they are integrated, more practical contact models can be built to describe a wide range of physical or engineering situations. Recently, in [22, 28], a rod–beam system is constructed to provide mathematical and numerical analyses on a V–shaped Micro-Electro-Mechanical Systems (MEMS) actuator.

In this work, we utilize two Kelvin–Voigt typed viscoelastic objects with the two contact conditions and a transmission condition to design a mechanical system. A nonlinear spring and a linear beam coalesce into a dynamic contact model to consider a spring–beam system which results in a system of differential equations with the three conditions aforementioned. This contact model can be regarded as a boundary thin deformable obstacle problem. The system consists of an initial–boundary value problem (IBVP) and an extended Duffing equation (see the book [3] for the original Duffing equation) with initial data. The Duffing equation written by a second order nonlinear ordinary differential equation (ODE) describes the motion of a viscoelastic spring. The IBVP which contains a couple of linear partial differential equations (PDEs) also describes the motion of a viscoelastic Timoshenko beam [11, 12]. Unlike most contact models, our contact model is considered by using both the normal compliance condition (see e.g., [13, 14] and references therein) and Signorini's condition. The first condition is for between one end of the beam and the top of the spring and the other is for when the spring is fully compressed and hits a rigid foundation. One can notice that the normal compliance is a regularization of

Received by the editors on February 4, 2022 and, accepted on September 24, 2022.
2000 *Mathematics Subject Classification.* 34A12, 35M33, 65J08, 74H15, 74H20.
*Corresponding author.

contact forces in Signorini's condition. A similar but simpler contact model can be found in [10]. In addition to the two contact conditions, a transmission condition is combined with the normal compliance condition, when the end of the beam and the top of the spring touch each other. In fact, the transmission condition is inspired by the model of a beam on Emil Winkler's elastic foundation, [2] published in 1867. His model has received special attention from civil engineering communities, since it has simple but profound assumptions. We note that the springs used in the Winkler's model are linearly elastic and that there are multiple contacts between a beam and the springs.

In many papers (e.g., [25, 26, 27, 24] and references therein), the Duffing equation is first modified and then the analytical solutions are found. In future work, the first author in this paper will generalize the Duffing equation more mathematically and then add dynamic frictional contact conditions formed by Coulomb's laws (see [8]). Due to the complexity of the problem, the solutions are unlikely to be found. Instead, its solvability will be studied and numerical schemes will be proposed.

In order to prove the existence results for the contact problem, we derive a corresponding variational formulation to the IBVP in the abstract setting and then apply Galerkin's method to it. Signorini's condition essentially causes nonsmooth solutions but the convolution of the standard mollifier and locally integrable solutions is employed to regularize them. While contact forces understood at the atomic level (see [1, Chapter I]) do not guarantee the conservation of energy or energy balance with viscosity, the regularized contact forces by means of the standard mollifier are likely to do so. Such a discrepancy will be explored in future work. We note that the regularization of the contact forces would be unrelated to the normal compliance condition.

We use a contraction mapping argument to prove the uniqueness of the solutions satisfying all the conditions except for Signorini's condition. We note that it still remains open to prove the uniqueness for Signorini's condition in the dynamic case.

The fully discrete numerical schemes are proposed, based on time discretizations on a time interval and finite element methods (FEMs) in the spacial domain. The overall scheme for computing each time step numerical approximations is to establish recursive relations and employ the the Newton–Raphson method. Particularly, block matrix manipulations and back substitutions are required to obtain the fully discrete numerical approximations of the PDEs. The Algorithm 1 presented in the section 5 explains all detailed steps. We also investigate numerical stability which is supported by numerical results, as we shall see them later.

This paper is organized as follows. The detailed illustrations for the mathematical model are presented in Section 2 and mathematical background is introduced in Section 3. In Section 4, we prove the existence of the global solutions in the continuous case. In Section 5, the fully discrete numerical schemes are explained and an algorithm is provided to compute numerical solutions. A criteria for numerical stability is also formed and validated. Several groups of data are chosen and then numerical simulations and results are presented and discussed in the last section 6.

2. A mathematical model

See Figure 1 to understand the dynamic contact model. An easiest way to understand the model is to consider the motion of seesaws at playgrounds. For a mathematical reason, we want to consider the motion of *a half* board which is described by a coupled PDEs (1–2). The half of the board is assume to be a linear

viscoelastic Timoshenko beam, in which its one end is clamped and another one touches the top of a nonlinear spring attached to the land. The governing equation of the spring is formed by an extended Duffing equation (6). The length of the beam is assumed to be one. Let $T > 0$ be the final time. For all $(t,\, x) \in [0,\, T] \times [0,\, 1]$ the vertical displacement and the rotatory angle of the beam are denoted by $u = u(t,\, x)$ and $\theta = \theta(t,\, x)$, respectively. The position of the spring's top is denoted by $y = y(t)$. The spring is assumed to be initially in the equilibrium state and let Ψ be its equilibrium position. When the one end of the beam hits the top of the spring, they start moving together and there occur contact forces between them, which are understood by the transmission condition in (7) and normal compliance condition in (5). The tip of the beam compresses the spring until it reaches to the land. The land is assumed to be a rigid foundation. The position of the land is denoted by φ. Then there happen contact forces, denoted by $N = N(t)$, which is understood by complementarity conditions (CCs) in (8). Thus, Signorini's condition can be alternatively interpreted by CCs: $0 \le a \perp b \ge 0$ means that either of a or b is zero. Based on the Winkler foundation model, we assume that the beam's tip and the top of the spring continue to be unseparated until they return to the equilibrium position of the spring. Finally, we assume that the beam moves down initially and it hits the top of the spring at a time $t = t_c \in (0,\, T]$.

According to the physical situation explained above, we are led to the following dynamic contact problem:

$$\begin{aligned}
&\rho I\theta_{tt} = E\,I\theta_{xx} + K\,A\,G\,(u_x - \theta)\\
&\qquad + \alpha_b E\,I\theta_{txx} + \alpha_b\,K\,A\,G\,(u_{tx} - \theta_t) \quad \text{in } (0,\, T] \times (0,\, 1), && (1)\\
&\rho A u_{tt} = K\,A\,G\,(u_{xx} - \theta_x) + \alpha_b\,K\,A\,G\,(u_{txx} - \theta_{tx}) + f_b \quad \text{in } (0,\, T] \times (0,\, 1), && (2)\\
&0 = u(t,\, 0) = \theta(t,\, 0) \quad \text{on } (0,\, T], && (3)\\
&0 = E\,I\theta_x(t,\, 1) + \alpha_b\,E\,I\theta_{tx}(t,\, 1) \quad \text{on } (0,\, T], && (4)\\
&\lambda_{nc}\,(\Psi - u(t,\, 1))_+^p = K\,A\,G\,(u_x(t,\, 1) - \theta(t,\, 1))\\
&\qquad + \alpha_b\,K\,A\,G\,(u_{tx}(t,\, 1) - \theta_t(t,\, 1)) \quad \text{on } (0,\, T], && (5)\\
&m\,y_{tt} + \alpha_s y_t + k_1\,y + k_2 y^3 = -\lambda_{nc}\,(\Psi - u(t,\, 1))_+^p + N(t) + f_s \quad \text{on } (t_c,\, T]\,, && (6)\\
&u(t,\, 1) = y(t) \quad \text{if } \varphi \le u(t,\, 1) \le \Psi \quad \text{on } (t_c,\, T]\,, && (7)\\
&0 \le N(t) \quad \perp \quad y(t) - \varphi \ge 0 \quad \text{on } (t_c,\, T]\,, && (8)\\
&\theta(0,\, x) = \theta^0(x), \quad \theta_t(0,\, x) = \theta_t^0(x) \quad \text{in } (0,\, 1), && (9)\\
&u(0,\, x) = u^0(x), \quad u_t(0,\, x) = u_t^0(x) \quad \text{in } (0,\, 1), && (10)\\
&y\,(t_c) = \Psi, \quad y_t\,(t_c) = \frac{1}{2}\left(u_t\left(t_c^-,\, 1\right) + u_t\left(t_c^+,\, 1\right)\right), \quad N(0) = 0, && (11)
\end{aligned}$$

where $f_b = f_b(t,\, x)$ and $f_s = f_s(t)$ are external body forces and all the initial data are given in (9–11). One can notice that the initial velocity of the spring in (11) is assumed to be the average of the left and right hand limits of the velocity of the beam's tip. All the coefficients are explained: ρ is the density of the beam, A is the area of its cross section, G is the modulus of elasticity of shear, K is the geometric dependent distribution of shear stress, E is Young modulus, I is the second moment of inertia, and m is the mass. In the Timoshenko beam theory, $E\,I$ represents the flexural rigidity of the beams. The essential boundary conditions are imposed in (3) and the natural boundary conditions are also imposed in (4–5). In the normal compliance condition, $\lambda_{nc} \ge 0$ and $p \ge 1$ are called the stiffness of a reactive spring and the normal compliance exponent, respectively. As we can see the subscripts

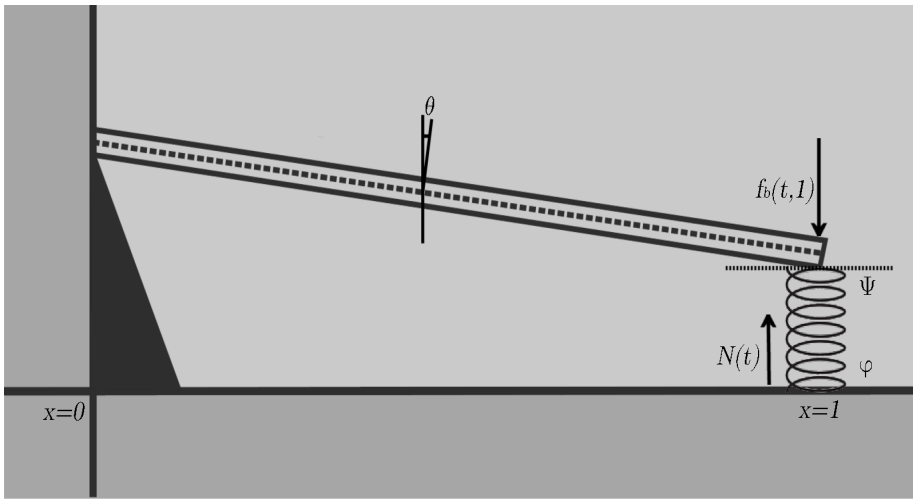

FIGURE 1. Physical setting.

of the solutions θ, u in (1–5), they indicate partial derivatives with respect to the subscripted variables. In addition, a subscript of the solution y in (6) means a time derivative.

3. Preliminaries

In this section, we provide the mathematical background to be able to prove the existence results for all the conditions (1–11). For mathematical conveniences, we assume that $\rho = I = E = K = A = G = m = 1$.

In this paper, vectors and matrices are denoted by bold-faced letters. For a sufficiently smooth vector–valued function, denoted by $\boldsymbol{u} = (\theta,\, u)^T : [0,\, 1] \to \mathbb{R}^2$, we define a differential operator $\mathcal{L}$:

$$\mathcal{L}\boldsymbol{u} = (\theta_{xx} + u_x - \theta,\, u_{xx} - \theta_x)\,.$$

Solution spaces for the contact problem are based on Gelfand triples: $V \subset H = H' \subset V'$. In this contact problem, $V = H_c^1\left(0,\, 1; \mathbb{R}^2\right)$ and $H = L^2\left(0,\, 1; \mathbb{R}^2\right)$. Here the subscript "$c$" means that one end of beams is clamped. Their alternative notations can be written as follows:

$$H_c^1\left(0,\, 1; \mathbb{R}^2\right) = H_L^1(0,\, 1) \times H_L^1(0,\, 1), \quad L^2\left(0,\, 1; \mathbb{R}^2\right) = L^2(0,\, 1) \times L^2(0,\, 1), \tag{12}$$

where $H_L^1(0,\, 1) = \left\{u \in H^1(0,\, 1) \mid u(0) = 0\right\}$. The subscript "$L$" means that the essential homogeneous boundary condition imposed at the the left of the beam. Thus, the Sobolev space $H_c^1\left(0,\, 1; \mathbb{R}^2\right)$ consists of vector–valued functions which satisfy the essential homogeneous boundary condition (3). For $\boldsymbol{v} = (\omega,\, v)^T$, $\boldsymbol{\varpi} = (\varpi,\, \nu)^T \in H$ the associate inner product on the space can defined to be

$$(\boldsymbol{v},\, \boldsymbol{\varpi})_H = \int_0^1 \omega\, \varpi + v\, \nu\, dx$$

and the associated norm can be easily defined. Similarly, the inner product and norm over the space V can be defined. Let X be a Banach space and X^* be a its dual space. Then the duality paring can be denoted by $\langle \cdot,\, \cdot \rangle_{X^* \times X}$. Assume that the vector–valued functions $\boldsymbol{g} = (g_1,\, g_2) \in X^*$ and $\boldsymbol{f} = (f_1,\, f_2)^T \in X$. Then the

duality pairing can be defined by

$$\langle \boldsymbol{g},\, \boldsymbol{f}\rangle_{\boldsymbol{X}^*\times\boldsymbol{X}} = \int_0^1 g_1 f_1 + g_2 f_2\, dx.$$

Let $\boldsymbol{u} \in V$ and $\boldsymbol{w} = (\vartheta,\, w)^T \in V$. Then we define an elliptic selfadjoint operator $\mathcal{A} : V \to V^*$:

$$\langle \mathcal{A}\boldsymbol{u},\, \boldsymbol{w}\rangle_{V^*\times V} := \int_0^1 \mathcal{L}\boldsymbol{u}\cdot\boldsymbol{w}\, dx = \int_0^1 \theta_x\vartheta_x + (u_x-\theta)\,(w_x-\vartheta)\, dx.$$

It is easy to see that the norm $\|\boldsymbol{u}\|_V$ is equivalent to $\sqrt{\langle \mathcal{A}\boldsymbol{u},\, \boldsymbol{u}\rangle}$. In addition, we can define the interpolation spaces $V_\sigma = H_L^\sigma(0,\,1)\times H_L^\sigma(0,\,1)$ for $\sigma\in\mathbb{R}$ with the associate norms $\|\cdot\|_{V_\sigma}$. Thus, it follows from the scales of the interpolation spaces that $V_0 = H$ and $V_1 = V$.

Let $\sigma = 1/2+\varepsilon$ with $\varepsilon > 0$. Then there is a bounded linear operator $\beta : H^\sigma(0,\,1)\to H^\varepsilon(1) = \mathbb{R}$, called the trace operator such that $\beta\, w = w(1)\in H^\varepsilon(1)$ for all $w\in H^\sigma(0,\,1)$. Here the notion of the space $H^\varepsilon(1)$ is that the functions w are restricted to the right boundary. Let $1\le q\le\infty$. Spaces involving time such as $L^q(0,\,T;X)$ or $W^{1,q}(0,\,T;X)$ with the associate norms can be easily defined and will be essential to construct the weak solutions to the PDEs.

Assume that $\boldsymbol{u} : [0,\,T]\times[0,\,1]\to\mathbb{R}^2$. Then, we use the trace operators and a projection operator from $V\to H^1(0,\,1)$ to define a composite operator $\mathcal{P} : V\to V^*$ by

$$\langle \mathcal{P}\boldsymbol{u},\, \boldsymbol{w}\rangle_{V^*\times V} = \lambda_{nc}\,(\Psi-\beta u\,(t))_+^p\,\beta\, w \quad \text{for } t\in[0,\,T], \tag{13}$$

where $\Psi\in\mathbb{R}$ is given and $(r)_+ = \max(r,\,0)$. We note that $\beta u(t,\,x)$ is replaced by $\beta u(t)$ for a simple notation.

In order to build approximations of functions on $\mathbb{R}$, we define the convolution operator, denoted by $*$, to be

$$f*g(t) = \int_{-\infty}^{\infty} f(t-s)g(s)\, ds = \int_{-\infty}^{\infty} f(s)g(t-s)\, ds.$$

The standard mollifier $\eta\in C^\infty$ is defined by

$$\eta\,(t) = \begin{cases} C\exp\left(\frac{1}{|t|^2-1}\right) & \text{if } |t|<1,\\ 0 & \text{if } |t|\ge 1.\end{cases}$$

Here the quantity $C>0$ is chosen such that $\int_{-\infty}^{\infty}\eta(t)\, dt = 1$.

As we shall see later, the simpler notations $\langle\cdot,\,\cdot\rangle$, $(\cdot,\,\cdot)$ will be used, if the choice of spaces is clear. Let $\boldsymbol{u}_t = \boldsymbol{v}$ and $y_t = z$. An energy functional in the continuous case is defined by

$$E(t) = E_b(t) + E_s(t), \tag{14}$$

where

$$E_b(t) := E_b\,[\boldsymbol{u}(t),\boldsymbol{v}(t)] = \frac{1}{2}\left((\boldsymbol{v},\,\boldsymbol{v}) + \langle \mathcal{A}\boldsymbol{u},\,\boldsymbol{u}\rangle\right) + \frac{\lambda_{nc}}{p+1}\,(\Psi-\beta\, u(t))_+^{p+1}$$

and

$$E_s(t) := E_s\,[z(t),y(t)] = \frac{1}{2}\left(z^2 + k_1y^2 + \frac{k_2}{2}y^4\right) - \frac{\lambda_{nc}}{p+1}\,(\Psi-y(t))_+^{p+1}.$$

One can notice that the total energy is $E(t) = E_b(\mathrm{t})$ if $t<t_c$ for an initial contact time t_c.

4. The existence results

In order to investigate a solvability of (1–11), we first derive a variational formulation (15) which corresponds to (1–5) and then present the following Problem 1.

Problem 1. Let $\boldsymbol{f}_b = (0,\, f_b)^T$. Assume that $\alpha_b,\, \alpha_s > 0$ and $(\boldsymbol{f}_b,\, f_s) \in L^2\,(0,\, T;\, L^2(0,\, 1) \times L^2(0,\, T)$. Find a solution $(\boldsymbol{u},\, y) : [0,\, T] \to V \times C[0,\, T]$ such that

$$\boldsymbol{v}_t = -\alpha_b \mathcal{A}\boldsymbol{v} - \mathcal{A}\boldsymbol{u} + \mathcal{P}\boldsymbol{u} + \boldsymbol{f}_b, \tag{15}$$

$$z_t = -\alpha_s z - k_1 y - k_2 y^3 - \lambda_{nc}\,(\Psi - \beta\, u(t))_+^p + N(t) + f_s, \tag{16}$$

$$\beta\, u(t) = y(t) \quad \text{if } \varphi \le \beta\, u(t) \le \Psi, \tag{17}$$

$$0 \le N(t) \quad \perp \quad y(t) - \varphi \ge 0, \tag{18}$$

$$\boldsymbol{u}(0,\, x) = \boldsymbol{u}^0 \in V, \quad \boldsymbol{v}(0,\, x) = \boldsymbol{v}^0 \in H, \tag{19}$$

$$y\,(t_c) = \Psi \in \mathbb{R}, \quad z(0) = \frac{1}{2}\left(u_t\left(t_c^-,\, 1\right) + u_t\left(t_c^+,\, 1\right)\right) \in \mathbb{R}, \quad N(0) = 0. \tag{20}$$

For the abstract variational formulation (15), we use Galerkin's method to choose sufficiently smooth functions $\phi_i = \phi_i(x)$ such that $\{\phi_i\}_{i=1}^{\infty}$ is an orthonormal basis of $L^2(0,\, 1)$ and is an orthogonal basis of $H_L^1(0,\, 1)$. In order to consider the solution spaces, we temporarily establish regularity assumptions that $(\boldsymbol{u},\, y) \in H^1\,(0,\, T; V) \times L^2_{\text{loc}}(0,\, T)$. Let $n \in \mathbb{N}$ to be sufficiently large. We assume that the solution of (15) is approximated by $\boldsymbol{u}^n : [0,\, T] \to V$ of the form

$$\boldsymbol{u}^n(t) = (\theta^n(t),\, u^n(t))^T = \left(\sum_{i=1}^{n} \theta_i(t)\phi_i(x),\, \sum_{i=1}^{n} u_i(t)\phi_i(x)\right)^T. \tag{21}$$

Similarly, we can write

$$\boldsymbol{v}^n(t) = (\omega^n(t),\, v^n(t))^T = \left(\sum_{i=1}^{n} \omega_i(t)\phi_i(x),\, \sum_{i=1}^{n} v_i(t)\phi_i(x)\right)^T.$$

The second order nonlinear DE (16) needs to be understood in the sense of distributions. We also employ the standard mollifier $\eta_{1/n}\,(t) := n\,\eta\,(n\,t)$ to approximate a solution y. We extend y to be 0 on the intervals $(-\infty,\, 0)$ and $(T,\, \infty)$. Then we set up approximations

$$y^n(t) = \eta_{1/n} * y\,(t) \quad \text{on } (1/n,\, T - 1/n).$$

The support of a function f is denoted by $\text{supp}(f) := \{t \in [0,\, T] \mid f(t) \neq 0\}$. Let $t_* \in (0,\, T)$ be an instantaneous contact time when the springs are fully compressed. In the CCs (25), the contact forces N are assumed to be approximated by

$$N^n(t) = \sum_{i=1}^{m} \eta_{1/n}\,(t - t_{*,i})\,,$$

where for each contact time $t_{*,i} \in (0,\, T]$ with $1 \le i \le m$

$$\int_0^T \eta_{1/n}\,(t - t_{*,i})\,dt = 1$$

and $\text{supp}\left(\eta_{1/n}\right) \subset (t_{*,i} - 1/n,\, t_{*,i} + 1/n)$ and $\eta_{1/n}\,(t - t_{*,i}) \to \delta\,(t - t_{*,i})$ as $n \uparrow \infty$. Here δ is the Dirac delta function (measure). Since n is sufficiently large, it is easy to see that $(t_{*,i} - 1/n,\, t_{*,i} + 1/n) \cap (t_{*,j} - 1/n,\, t_{*,j} + 1/n) = \emptyset$, if $i \neq j$.

Now, the main results of the existence are presented in the following Theorem 2.

Theorem 2. *Let $\alpha_b,\ \alpha_s > 0$ and $\varepsilon = 1/2$. Assume that $(\boldsymbol{f}_b,\ f_s) \in L^2\left(0,\ T; L^2(0,\ 1)\right) \times L^2\left(0,\ T\right)$. Then there is a solution $(\theta,\ u)$ and $(y,\ z)$ of (15–20) such that*

$$\begin{aligned}
\theta &\in C\left([0,\ T]\,; H_L^1(0,\ 1)\right) \cap W^{1,\infty}\left(0,\ T; L^2(0,\ 1)\right) \\
&\quad \cap H^1\left(0,\ T; H_L^1(0,\ 1)\right) \cap \left(C[0,\ T] \times C[0,\ 1]\right), \\
u &\in C\left([0,\ T]\,; H_L^1(0,\ 1)\right) \cap W^{1,\infty}\left([0,\ T]\,; L^2(0,\ 1)\right) \\
&\quad \cap H^1\left(0,\ T; H_L^1(0,\ 1)\right) \cap \left(C[0,\ T] \times C[0,\ 1]\right), \\
(y,\ z) &\in C\left[0,\ T\right] \times L^\infty\left(0,\ T\right).
\end{aligned}$$

Note that we can naturally extend the solutions $(y,\ z)$ to become the functions $y(t) = \Psi$ and $z(t) = 0$ for $t \in [0,\ t_c)$.

First, we want to seek the approximations $(\boldsymbol{u}^n,\ y^n)$ for a sufficiently large $n \in \mathbb{N}$ in some Banach spaces involving time such that

$$\boldsymbol{v}_t^n = -\alpha_b \mathcal{A}\boldsymbol{v}^n - \mathcal{A}\boldsymbol{u}^n + \mathcal{P}\boldsymbol{u}^n + \boldsymbol{f}_b, \tag{22}$$

$$z_t^n = -\alpha_s z^n - k_1 y^n - k_2 \left(y^n\right)^3 - \lambda_{nc}\left(\Psi - \beta\, u^n(t)\right)_+^p + N^n(t) + f_s, \tag{23}$$

$$\beta\, u^n(t) = y^n(t) \quad \text{if } \varphi \le \beta\, u^n(t) \le \Psi, \tag{24}$$

$$0 \le N^n(t) \quad \perp \quad y^n(t) - \varphi \ge 0, \tag{25}$$

$$\theta_i(0) = \left(\theta^0,\ \phi_i\right), \quad u_i(0) = \left(u^0,\ \phi_i\right), \tag{26}$$

$$\omega_i(0) = \left(\omega^0,\ \phi_i\right), \quad v_i(0) = \left(v^0,\ \phi_i\right), \tag{27}$$

$$y^n\left(t_c\right) = \Psi \in \mathbb{R}, \quad z^n(0) = \frac{1}{2}\left(\beta\, v^n\left(t_c^-\right) + \beta\, v^n\left(t_c^+\right)\right) \in \mathbb{R}, \quad N^n(0) = 0. \tag{28}$$

Now, we consider a validation for construction of the approximations in (21) satisfying (22) and (26–27). Define the following four bilinear forms: for $(\theta,\ u)^T,\ (\vartheta,\ w)^T \in V$

$$\begin{aligned}
a_{11}(\theta,\ \vartheta) &= (\theta_x,\ \vartheta_x) + (\theta,\ \vartheta), \quad a_{12}\left(u,\ w\right) = -\left(u_x,\ w\right), \\
a_{21}\left(\theta,\ \vartheta\right) &= \left(\theta,\ \vartheta_x\right), \quad a_{22}\left(u,\ w\right) = -\left(u_x,\ w_x\right),
\end{aligned}$$

where $(\cdot,\ \cdot)$ denotes the inner product in $L^2(0,\ 1)$. From (22) we can derive the following second order ODE system easily: for each $1 \le i \le n$

$$\begin{aligned}
\begin{bmatrix} \ddot{\theta}_i(t) \\ \ddot{u}_i(t) \end{bmatrix} &= -\alpha_b \begin{bmatrix} a_{11}\left(\phi_i,\ \phi_j\right) & a_{12}\left(\phi_i,\ \phi_j\right) \\ a_{21}\left(\phi_i,\ \phi_j\right) & a_{22}\left(\phi_i,\ \phi_j\right) \end{bmatrix} \begin{bmatrix} \dot{\theta}_j(t) \\ \dot{u}_j(t) \end{bmatrix} \\
&\quad - \begin{bmatrix} a_{11}\left(\phi_i,\ \phi_j\right) & a_{12}\left(\phi_i,\ \phi_j\right) \\ a_{21}\left(\phi_i,\ \phi_j\right) & a_{22}\left(\phi_i,\ \phi_j\right) \end{bmatrix} \begin{bmatrix} \theta_j(t) \\ u_j(t) \end{bmatrix} + \begin{bmatrix} 0 \\ d_j(t) \end{bmatrix} + \begin{bmatrix} 0 \\ \left(f_b(t),\ \phi_i\right) \end{bmatrix},
\end{aligned} \tag{29}$$

where

$$d_i(t) = \lambda_{nc}\left(\Psi - u_j(t)\right)_+^p \beta\, \phi_j\, \beta\, \phi_i. \tag{30}$$

Note that the Einstein summation notation is used in (29–30) and $\dot{(\,)}$, $\ddot{(\,)}$ in (29) are the first and second time derivatives, respectively. We intend to determine all the coefficients $(\theta_i,\ u_i)$ for $1 \le i \le n$ to satisfy (22) and (26–27). Let $\boldsymbol{u}_i = \boldsymbol{u}_i(t) = (\theta_i(t),\ u_i(t))$ for each $i \in \mathbb{N}$. Then the nonlinear ODE (29) can be consider in the following vector equation

$$\ddot{\boldsymbol{u}}_i = \boldsymbol{F}\left(t,\ \boldsymbol{u}_i,\ \dot{\boldsymbol{u}}_i\right). \tag{31}$$

See the book [4, Sec 1.6]. Since $\left(\Psi - u_j(t)\right)_+^p$ is Lipschitz, the vector function $\boldsymbol{F}$ in (31) is Lipschitz as well and thus we can guarantee only local uniqueness and

existence of the solution $\boldsymbol{u}_i$. However, we will use a priori energy estimates and then pass to the limits as $n \uparrow \infty$, which enables us to prove that there is a unique weak solution satisfying (22) and (26–27) on the global time interval $[0,\, T]$.

Throughout this paper, $C > 0$ is a fixed quantity and may be different in each occurrence. In the following Lemma 3, based on some estimates, we show the uniform boundedness of the approximations for a sufficiently large $n \in \mathbb{N}$.

Lemma 3. *Let $\alpha_b,\, \alpha_s > 0$. Assume that $(f_b,\, f_s) \in L^2\left(0,\, T; L^2(0,\, 1)\right) \times L^2(0,\, T)$ and $E(0) \le M < \infty$. Then $(\boldsymbol{u}^n,\, y^n)$ and $(\boldsymbol{v}^n,\, z^n)$ satisfying (22–28) are uniformly bounded in $C\left([0,\, T]\,; V\right) \times C\left[0,\, T\right]$ and $\left(L^\infty(0,\, T; H) \cap L^2(0,\, T; V)\right) \times L^\infty\left(0,\, T\right)$ for sufficiently large $n \in \mathbb{N}$, respectively. $\boldsymbol{v}_t^n$ is also uniformly bounded in $L^2\left(0,\, T; V^*\right)$ for a sufficiently large $n \in \mathbb{N}$.*

Proof. For our convenient notations, the approximations $\boldsymbol{u}^n$ and $\boldsymbol{v}^n$ are denoted by $\boldsymbol{u}$ and $\boldsymbol{v}$, respectively. We take the inner product with $\boldsymbol{v} \in H^1\left(0,\, T; V\right)$ on both sides of (15). Then it is easy to see that for a. a. $t \in (0,\, T]$

$$\frac{1}{2}\int_0^t \frac{d}{d\tau}\left(\boldsymbol{v},\, \boldsymbol{v}\right) d\tau + \alpha_b \int_0^t \left\langle \mathcal{A}\boldsymbol{v}, \boldsymbol{v}\right\rangle d\tau + \frac{1}{2}\int_0^t \frac{d}{d\tau}\left\langle \mathcal{A}\boldsymbol{u}, \boldsymbol{u}\right\rangle d\tau - \int_0^t \left\langle \mathcal{P}\boldsymbol{u},\, \boldsymbol{v}\right\rangle d\tau$$

(32)

$$= \int_0^t \left(\boldsymbol{f}_b,\, \boldsymbol{v}\right) d\tau.$$

We recall (13) to see that the last integral in the left side of (15) becomes

$$\int_0^t \left\langle \mathcal{P}\boldsymbol{u},\, \boldsymbol{v}\right\rangle d\tau = -\frac{\lambda_{nc}}{p+1}\int_0^t \frac{d}{d\tau}\left(\Psi - \beta\, u(\tau)\right)_+^{p+1} d\tau. \tag{33}$$

Thus it follows from (32) and (33) that

$$E_b(t) + \alpha_b \int_0^t \left\langle \mathcal{A}\boldsymbol{v}, \boldsymbol{v}\right\rangle d\tau \le E_b(0) + \int_0^t \left(\boldsymbol{f}_b,\, \boldsymbol{v}\right) d\tau. \tag{34}$$

y^n, z^n, and N^n are also denoted by y, z, and N, respectively. Multiply both sides in (23) by z to see that

$$\begin{aligned}
&\frac{1}{2}\left(\int_0^t \frac{d}{d\tau}\left[z(\tau)\right]^2 + k_1 \frac{d}{d\tau}\left[y(\tau)\right]^2 + \frac{k_2}{2}\frac{d}{d\tau}\left[y(\tau)\right]^4\right) d\tau \\
&\quad + \alpha_s \int_0^t \left[z(\tau)\right]^2 d\tau - \int_0^t N(\tau)\frac{d}{d\tau}\left(y(\tau) - \varphi\right) d\tau \\
&\quad + \int_0^t \lambda_{nc}\left(\Psi - y(\tau)\right)_+^p \frac{d}{d\tau}\left(y(\tau) - \Psi\right) d\tau = \int_0^t f_s(\tau)\, z(\tau)\, d\tau.
\end{aligned} \tag{35}$$

Note that y will be a trivial solution over $[0,\, t_c)$. Thus we can obtain

(36)

$$E_s(t) + \alpha_s \int_0^t \left[z(\tau)\right]^2 d\tau - \int_0^t N(\tau)\frac{d}{d\tau}\left(y(\tau) - \varphi\right) d\tau \le E_s(0) + \int_{t_c}^t f_s(\tau)\, z(\tau)\, d\tau$$

We add (34) into (36) to see from (24) that

$$\begin{aligned}
&E(t) + \alpha_b \int_0^t \left\langle \mathcal{A}\boldsymbol{v}, \boldsymbol{v}\right\rangle d\tau + \alpha_s \int_0^t \left[z(\tau)\right]^2 d\tau - \int_0^t N(\tau)\frac{d}{d\tau}\left(y(\tau) - \varphi\right) d\tau \\
&\le E(0) + \int_0^t \left(\boldsymbol{f}_b,\, \boldsymbol{v}\right) d\tau + \int_0^t f_s(\tau) z(\tau)\, d\tau.
\end{aligned} \tag{37}$$

We use integration by parts and the CCs in (25) to see easily that

$$\int_0^t N(\tau)\frac{d}{d\tau}\left(y(\tau)-\varphi\right)d\tau = \int_0^t \left(y(\tau)-\varphi\right)\frac{d}{d\tau}N(\tau)\,d\tau = 0.$$

Thus it follows from (37) that

$$E(t)+\alpha_b\int_0^t \langle \mathcal{A}\boldsymbol{v},\boldsymbol{v}\rangle\,d\tau+\alpha_s\int_0^t [z(\tau)]^2\,d\tau \le E(0)+\int_0^t (\boldsymbol{f}_b,\,\boldsymbol{v})\,d\tau+\int_0^t f_s z\,d\tau. \tag{38}$$

Now we can use Cauchy's inequality to have

$$E(t) \le E(0)+\frac{1}{2}\left(\|f_b\|^2_{L^2(0,\,T;L^2(0,\,1))}+\|f_s\|^2_{L^2(0,\,T)}\right)+\frac{1}{2}\int_0^t \|v\|^2_{L^2(0,\,1)}+z^2 d\tau. \tag{39}$$

Recall the energy function (14). Let $g(t)=\|v(t)\|^2_{L^2(0,\,1)}+[z(t)]^2$. Then can easily see that

$$g(t) \le \int_0^t g(t)d\tau + C,$$

where $C=E(0)+\|f_b\|^2_{L^2(0,\,T;L^2(0,\,1))}+\|f_s\|^2_{L^2(0,\,T)}$. Gronwall's inequality allows us to have

$$\|v(t)\|^2_{L^2(0,\,1)}+[z(t)]^2 \le C\left(1+Te^T\right) \quad \text{for a.a. } t\in[0,\,T].$$

Thus, it is straightforward to see from (38) and (39) that $(\boldsymbol{u}^n,\,y^n)$ is uniformly bounded in $C\left([0,\,T]\,;V\right)\times C\left[0,\,T\right]$ and $(\boldsymbol{v}^n,\,z^n)$ is uniformly bounded in $(L^\infty(0,\,T;H)$ $\cap L^2(0,\,T;V)\times L^\infty\left(0,\,T\right)$ for any $n\ge 1$.

Multiply (22) by $\boldsymbol{w}\in V$ with $\|\boldsymbol{w}\|_V \le 1$ in (32). Then it is easy to see that

$$|\langle \ddot{\boldsymbol{u}},\boldsymbol{w}\rangle| \le C\left(\|f_b\|_{L^2(0,1)}+\|\boldsymbol{u}\|_V+\|\boldsymbol{v}\|_V\right).$$

Thus we can have

$$\int_0^T \|\ddot{\boldsymbol{u}}\|^2_{V^*}\,dt \le C\left(E(0)+\|f_b\|^2_{L^2(0,\,T;L^2(0,\,1))}+\|f_s\|^2_{L^2(0,\,T)}\right)$$

which implies that $\ddot{\boldsymbol{u}}^n$ is uniformly bounded in $L^2\left(0,\,T;V^*\right)$. The proof is complete now. □

We use the previous Lemma 3 to show that there is a weak solution of (22) and (26–27). From now on, the strong, weak, and weak* convergences are denoted by $\to$, $\rightharpoonup$, and $\rightharpoonup^*$, respectively.

Lemma 4. *There exists a weak solution $\boldsymbol{u}\in H^1(0,\,T;V)$ satisfying the conditions (15) and (19).*

Proof. It follows from the previous Lemma 3 that approximations $\boldsymbol{u}^n$ and $\ddot{\boldsymbol{u}}^n$ are bounded in $H^1\left(0,\,T;V\right)$ and $L^2\left(0,\,T;V^*\right)$ for any $n\ge 1$, respectively. Thus there are their corresponding subsequences, denoted by $\{\boldsymbol{u}^{n_l}\}$, $\{\ddot{\boldsymbol{u}}^{n_l}\}$ such that

$$\begin{aligned} &\boldsymbol{u}^{n_l} \rightharpoonup \boldsymbol{u} \quad \text{in } H^1\left(0,\,T;V\right) \text{ and} \\ &\ddot{\boldsymbol{u}}^{n_l} \rightharpoonup \ddot{\boldsymbol{u}} \quad \text{in } L^2\left(0,\,T;V^*\right), \end{aligned} \tag{40}$$

as $l\to\infty$. We restrict our attention to those subsequences. Choose any test functions $\boldsymbol{w}\in\mathcal{W}$, where

$$\mathcal{W}=\left\{\boldsymbol{w}\in C^2(0,T;V)\mid \boldsymbol{w}(T)=\dot{\boldsymbol{w}}(T)=0\right\}.$$

Let $n = n_l$ for our convenience. Then we take the inner product on both sides of (22) with $\boldsymbol{w}$ and take integrals with respect to $t \in (0,\, T]$ to see that

$$\begin{aligned}\int_0^T (\ddot{\boldsymbol{u}}^n,\, \boldsymbol{w})\, dt = &- \int_0^T \alpha_b \left\langle \mathcal{A}\boldsymbol{v}^n,\, \boldsymbol{w}\right\rangle + \left\langle \mathcal{A}\boldsymbol{u}^n,\, \boldsymbol{w}\right\rangle dt \\ &+ \int_0^T \left\langle \mathcal{P}\boldsymbol{u}^n,\, \boldsymbol{w}\right\rangle dt + \int_0^T (\boldsymbol{f}_b,\, \boldsymbol{w})\, dt. \end{aligned} \tag{41}$$

We pass the approximations to the limits. Then it is easy to see from (40) that

$$\int_0^T (\ddot{\boldsymbol{u}},\, \boldsymbol{w})\, dt = - \int_0^T \alpha_b \left\langle \mathcal{A}\boldsymbol{v},\, \boldsymbol{w}\right\rangle + \left\langle \mathcal{A}\boldsymbol{u},\, \boldsymbol{w}\right\rangle dt + \int_0^T \left\langle \mathcal{P}\boldsymbol{u},\, \boldsymbol{w}\right\rangle dt + \int_0^T (\boldsymbol{f}_b,\, \boldsymbol{w})\, dt. \tag{42}$$

Thus the variational formulation (15) holds for all $\boldsymbol{w} \in V$ and almost all $t \in (0,\, T]$. Now we claim that the solution $\boldsymbol{u}$ satisfies the two initial data (19). We apply integration by parts twice in (41) and (42). Then we can obtain the following identity

$$-\left(\boldsymbol{u}^n(0),\, \dot{\boldsymbol{w}}(0)\right) + \left(\boldsymbol{v}^n(0),\, \boldsymbol{w}(0)\right) = -\left(\boldsymbol{u}^0,\, \dot{\boldsymbol{w}}(0)\right) + \left(\boldsymbol{v}^0,\, \boldsymbol{w}(0)\right).$$

Since $\boldsymbol{w}(0)$ and $\dot{\boldsymbol{w}}(0)$ are arbitrary, the initial conditions imposed by the weak solution $\boldsymbol{u}$ hold. The proof is complete now. □

In the next Lemma 5, we use a contraction mapping argument to show the uniqueness of the solutions satisfying all the conditions considered in the Problem 1 except the CCs in (18). We note that proving the uniqueness of solutions satisfying the CCs is an open question. Since the solutions $\boldsymbol{u} \in H^1(0,\, T; V)$ and $(y,\, z) \in C\left[t_c,\, T\right] \times L^\infty\left(t_c,\, T\right)$, we can write

$$\boldsymbol{u}(t) = \boldsymbol{u}(s) + \int_s^t \boldsymbol{v}(\tau)\, d\tau, \quad y(t) = y(s) + \int_s^t z(\tau)\, d\tau \tag{43}$$

for $t_c \le s \le t \le T$.

Lemma 5. *There is a unique weak solution* $(\boldsymbol{u},\, y)$ *satisfying (15–17) and (19–20), provided that* $N(t) = 0$ *for* $t \in [0,\, T]$.

Proof. Assume that there are two solutions $(\boldsymbol{u}_1, y_1)$ and $(\boldsymbol{u}_2, y_2) \in C([0,\, T]; V) \times C[0,\, T]$ satisfying (15–17) and (19–20). Let $\boldsymbol{u} = \boldsymbol{u}_1 - \boldsymbol{u}_2$ and thus $\boldsymbol{v} = \dot{\boldsymbol{u}}_1 - \dot{\boldsymbol{u}}_2$. Also let $y = y_1 - y_2$ and thus $z = \dot{y}_1 - \dot{y}_2$. Note that we do not want to consider the trivial solutions y_1 and y_2, if $t \in [0,\, t_c)$. Now, we claim that $(\boldsymbol{u}, y)$=$\boldsymbol{0}$, if $N(t) = 0$. If $\lambda_{nc} = 0$, it is straightforward to show the uniqueness of (15). If $\lambda_{nc} > 0$, then we first show that $\boldsymbol{u}(t) = \boldsymbol{0}$ for $t \in [0,\, T]$. Since the initial data (19) are shared, it is easy to see from (15) that over a local interval $\left[0,\, t_1^b\right] \subset [0,\, T]$

$$\frac{1}{2}\left(\left\|\boldsymbol{v}\left(t_1^b\right)\right\|_H^2 + \left\|\boldsymbol{u}\left(t_1^b\right)\right\|_V^2\right) + \alpha_b \int_0^{t_1^b} \|\boldsymbol{v}(\tau)\|_V^2\, d\tau = \int_0^{t_1^b} \left\langle \mathcal{P}\boldsymbol{u}_1 - \mathcal{P}\boldsymbol{u}_2,\, \boldsymbol{v}\right\rangle d\tau. \tag{44}$$

Note that t_1^b will be small enough, as we shall see later. Recall (13). Since $(\cdot)_+^p$ is Lipschitz, we can use the trace theorem and Cauchy's inequality with $\epsilon > 0$ to obtain

$$\begin{aligned}\int_0^{t_1^b} \left\langle \mathcal{P}\boldsymbol{u}_1 - \mathcal{P}\boldsymbol{u}_2,\, \boldsymbol{v}\right\rangle d\tau &= \lambda_{nc} \int_0^{t_1^b} \left(\left(\Psi - \beta u_1\left(\tau\right)\right)_+^p - \left(\Psi - \beta u_2\left(\tau\right)\right)_+^p\right) \beta\, v\, d\tau \\ &\le C \int_0^{t_1^b} \frac{1}{\epsilon} \|u\|_{H_L^1(0,\,1)}^2 + \epsilon \|v\|_{H_L^1(0,\,1)}^2\, d\tau. \end{aligned} \tag{45}$$

Thus, we combine (45) with (44) to have

$$\begin{aligned}&\frac{1}{2}\left(\left\|\boldsymbol{v}\left(t_1^b\right)\right\|_H^2+\left\|\boldsymbol{u}\left(t_1^b\right)\right\|_V^2\right)+\alpha_b\int_0^{t_1^b}\|\omega(\tau)\|_{H_L^1(0,\,1)}^2\,d\tau\\&\quad+\left(\alpha_b-C\epsilon\right)\int_0^{t_1^b}\|v(\tau)\|_{H_L^1(0,\,1)}^2\,d\tau\leq\frac{C}{\epsilon}\int_0^{t_1^b}\|u(\tau)\|_{H_L^1(0,\,1)}^2\,d\tau.\end{aligned}\tag{46}$$

Now we can choose a sufficiently small $\epsilon>0$ such that $\alpha_b-C\epsilon>0$. We define the norm on the local interval to be

$$\|u(t)\|_{L^\infty\left(0,\,t_1^b;H_L^1(0,\,1)\right)}=\max_{0\leq t\leq t_1^b}\|u(t)\|_{H_L^1(0,\,1)}.$$

We recall (43). We use Hölder's inequality to see that for $t\in\left[0,\,t_1^b\right]$

$$\|u\left(t\right)\|_{H_L^1(0,\,1)}\leq\int_0^t\|v\left(\tau\right)\|_{H_L^1(0,\,1)}\,d\tau\leq\sqrt{t_1^b}\left(\int_0^{t_1^b}\|v(\tau)\|_{H_L^1(0,\,1)}^2\,d\tau\right)^{1/2}.\tag{47}$$

Thus, it follows from (46–47) that

$$\|u(t)\|_{L^\infty\left(0,\,t_1;H_L^1(0,\,1)\right)}\leq t_1^b\sqrt{\frac{C}{\left(\alpha_b-C\epsilon\right)\epsilon}}\,\|u(t)\|_{L^\infty\left(0,\,t_1;H_L^1(0,\,1)\right)}.\tag{48}$$

We also choose a sufficiently small $t_1^b>0$ such that $t_1^b\sqrt{C/\left(\alpha_b-C\epsilon\right)\epsilon}<1$. We can see from (48) that $u(t)=0$ on $\left[0,\,t_1^b\right]$. Similarly, the estimate (46) allows us to have

$$\|\theta\left(t\right)\|_{H_L^1(0,\,1)}\leq\int_0^t\|\omega\left(\tau\right)\|_{H_L^1(0,\,1)}\,d\tau\leq\sqrt{t_1^b}\left(\int_0^{t_1^b}\|\omega(\tau)\|_{H_L^1(0,\,1)}^2\,d\tau\right)^{1/2}=0,$$

which implies that $\theta(t)=0$ on $\left[0,\,t_1^b\right]$. We continue to apply the same argument on the next local intervals $\left[t_1^b,\,t_2^b\right]$, $\left[t_2^b,\,t_3^b\right]$, etc. to prove that $\boldsymbol{u}(t)=\boldsymbol{0}$ on $[0,\,T]$.

Now, we turn to show that $y(t)=0$ for each $t\in[0,\,T]$. Let $[0,\,t_1^s]\subset[0,\,T]$. Since there is a unique solution $\boldsymbol{u}$, the transmission condition in (17) and the similar argument above and several algebraic manipulations allow us to have

$$\begin{aligned}&\frac{1}{2}\left(\left[z\left(t_1^s\right)\right]^2+k_1\left[y\left(t_1^s\right)\right]^2\right)+\alpha_s\int_{t_c}^{t_1^s}\left[z(\tau)\right]^2d\tau\\=&-k_2\int_0^{t_1^s}\left(\left(y_1(\tau)\right)^3-\left(y_2(\tau)\right)^3\right)z(\tau)d\tau\\&-\lambda_{nc}\int_0^{t_1^s}\left(\left(\Psi-y_1\left(\tau\right)\right)_+^p-\left(\Psi-y_2\left(\tau\right)\right)_+^p\right)z\,d\tau\leq C\int_0^{t_1^s}\left|y(\tau)\,z(\tau)\right|d\tau\\&\leq C\int_0^{t_1^s}\frac{1}{\epsilon}\left|y(\tau)\right|^2+\epsilon\left|z(\tau)\right|^2d\tau.\end{aligned}$$

By the similar argument to the beam equation, we can prove that obtain $y(t)=0$ on $[0,\,t_1^s]$. But we choose $t_i=\min\left(t_i^b,\,t_i^s\right)$ for $i\geq1$ to validate the contraction mapping argument for the entire differential equation system. Consequently, we apply the same argument on the next local intervals $[t_1,\,t_2]$, $[t_2,\,t_3]$, etc. to show the uniqueness of the solutions on $[0,\,T]$. The proof is now complete. □

We can observe from the previous Lemma 3 that $\|\boldsymbol{v}(t)\|_H$ and $\|\boldsymbol{u}(t)\|_V$ are uniformly bounded for almost all $t \in [0,\, T]$. Thus it follows that for $s,\, t \in [0,\, T]$

$$\|\boldsymbol{u}(t) - \boldsymbol{u}(s)\|_H \leq \int_s^t \|\boldsymbol{v}(\tau)\|_H \, d\tau \leq C|t-s|.$$

We use the interpolation space inequality (e.g., see the book [5, Theorem 1.3.3(g)]): $\|\boldsymbol{u}\|_{V_\sigma} \leq C_\sigma \|\boldsymbol{u}\|_H^{1-\sigma} \|\boldsymbol{u}\|_V^{\sigma}$, where $1 \leq \sigma \leq 1$. So it is easy to see that

$$\|\boldsymbol{u}(t) - \boldsymbol{u}(s)\|_{V_\sigma} \leq C_\sigma |t-s|^{1-\sigma}.$$

Let $\rho = 1 - \sigma$ with $0 \leq \sigma < 1$. We can apply Sobolev embedding theorem and Arzella–Ascoli theorem to see that $C^\rho\,(0,\, T; V_\sigma)$ with $1/2 < \sigma < 1$ are compactly embedded in $C[0,\, T] \times C[0,\, 1]$.

In the following Lemma 6, we prove that the limits of $(y^n,\, N^n)$ satisfy the CCs (18) in the weak sense.

Lemma 6. *There are subsequences $(y^n,\, N^n)$ such that $N^n \rightharpoonup^* N$, $y^n \to y$. The solutions satisfy the CCs (18) in the weak sense.*

Proof. Recall from the previous Lemma 3 that (y^n, z^n) are uniformly bounded in $C\,[0,\, T] \times L^2\,(0,\, T)$ for sufficiently large n. We take integrals on both sides of (23) to see that

$$\begin{aligned}\int_0^T N^n(t)\, dt &\leq |z^n(T)| + |z^n(0)| + \alpha_s \int_0^T |z^n(t)|\, dt \\ &\quad + k_1 \int_0^T |y^n(t)|\, dt + k_2 \int_0^T |y^n(t)|^3\, dt + \sqrt{T}\, \|f\|_{L^2(0,\, T)} \leq M < \infty. \end{aligned} \tag{49}$$

Since N^n can be identified with the Borel measure $\int_{t_c}^T N^n(t)\, dt$ by Riesz representation theorem, we can use Alaoglu's theorem to see that there is a subsequence, denoted by $\{N^n\}$, such that $N^n \rightharpoonup^* N$ as measures. We note that we keep using the same notation $\{N^n\}$ for our convenience. We take a sequence $\{y^n\}$ such that $y^n \to y$ in $C\,[0,\, T]$, as $n \uparrow \infty$. $\{y^n\}$ is assumed to correspond to $\{N^n\}$. Since $N^n \geq 0$ $y^n - \varphi \geq 0$, clearly $N \geq 0$ and $y - \varphi \geq 0$. It is also easy to see that

$$0 = \int_0^T N^n(t)\, (y^n(t) - \varphi)\, dt \to \int_0^T N(t)\, (y(t) - \varphi)\, dt,$$

as required. □

5. The fully discrete numerical schemes

In order to propose the fully discrete numerical schemes, we employ a time discretization and FEM, where the time step size and the size of subintervals, denoted by $h_t > 0$ and $h_x > 0$ respectively are accompanied. The number of time steps and the number of subintervals are also denoted by $P_t = \lfloor T/h_t \rfloor$ and $P_s = \lfloor 1/h_x \rfloor$, respectively. Then the space $[0,\, T] \times [0,\, 1]$ will be uniformly partitioned:

$$\begin{aligned} 0 = t_0 < t_1 < \cdots < t_l < \cdots < t_{P_t - 1} < t_{P_t} = T, \\ 0 = x_0 < x_1 < \cdots < x_i < \cdots < x_{P_s - 1} < x_{P_s} = 1, \end{aligned}$$

where each time step $t_l = l\, h_t$ for $0 \leq l \leq P_t$ and each node $x_i = i\, h_x$ for $0 \leq i \leq P_s$. We assume that $t_c \in \{t_l \mid 0 \leq l \leq P_t\}$. The fully discrete numerical solutions for $(\boldsymbol{u},\, \boldsymbol{v},\, y,\, z,\, N)$ are denoted by $(\boldsymbol{u}_{h_t,h_x},\, \boldsymbol{v}_{h_t,h_x},\, y_{h_t},\, z_{h_t},\, N_{h_t})$ and thus we can write

$$\begin{aligned} &(\boldsymbol{u}\,(t_l,\, x_i)\,.\boldsymbol{v}\,(t_l,\, x_i)\,,\, y\,(t_l)\,,\, z\,(t_l)\,,\, N\,(t_l)) \\ &\quad \approx (\boldsymbol{u}_{h_t,h_x}\,(t_l,\, x_i)\,,\, \boldsymbol{v}_{h_t,h_x}\,(t_l,\, x_i)\,,\, y_{h_t}\,(t_l)\,,\, z_{h_t}\,(t_l)\,,\, N_{h_t}\,(t_l)) \end{aligned}$$

for the sufficiently small parameters h_t, h_x.

First, we use a FEM in the spacial domain [0, 1] to obtain semi discrete approximations for Timoshenko beam equation. Let $I_i = [x_{i-1},\, x_i]$ with $1 \le i \le P_s$. Then a finite dimensional space can be defined by

$$V_{h_x} = \left\{ (\theta_{h_x}, u_{h_x}) \in V \mid \left(\theta_{h_x}|_{I_i},\ u_{h_x}|_{I_i} \right) \in \mathcal{P}_1(I_i) \times \mathcal{P}_1(I_i),\ 1 \le i \le P_s \right\},$$

where $\mathcal{P}_1(I_i)$ is a collection of linear functions on the subinterval I_i. A basis function $\psi_i(x)$ with $1 \le i \le P_s$ is constructed by a typical piecewise linear function on a subinterval $[x_{i-1},\, x_{i+1}]$. Now $(\boldsymbol{u}_{h_t,h_x},\, \boldsymbol{v}_{h_t,h_x})$ at each time step $t = t_l$ is written to be

$$\boldsymbol{u}_{h_t,h_x}(t_l,\, x) := \boldsymbol{u}^l_{h_x}(x) = \left(\sum_{j=1}^{P_s} \theta^l_j \psi_j(x),\, \sum_{j=1}^{P_s} u^l_j \psi_j(x) \right), \tag{50}$$

$$\boldsymbol{v}_{h_t,h_x}(t_l,\, x) := \boldsymbol{v}^l_{h_x}(x) = \left(\sum_{j=1}^{P_s} \omega^l_j \psi_j(x),\, \sum_{j=1}^{P_s} v^l_j \psi_j(x) \right). \tag{51}$$

where $\psi_j(x_i) = \delta_{ij}$. Note that δ_{ij} is the Kronecker delta function. Thus the fully discrete numerical approximations at each time step $t = t_l$ and node x_i are denoted by

$$\widetilde{\theta}^l = \left(\theta^l_1, \theta^l_2, \cdots, \theta^l_{P_s}\right)^T, \quad \widetilde{\omega}^l = \left(\omega^l_1, \omega^l_2, \cdots, \omega^l_{P_s}\right)^T,$$
$$\widetilde{u}^l = \left(u^l_1, u^l_2, \cdots, u^l_{P_s}\right)^T, \quad \widetilde{v}^l = \left(v^l_1, v^l_2, \cdots, v^l_{P_s}\right)^T.$$

Next, a time discretization is combined with the FEM. On local time intervals $[t_l,\, t_{l+1}]$, we use a piecewise linear interpolant $(\boldsymbol{u}_{h_t,h_x},\, y_{h_t})$ such that

$$\left(\boldsymbol{u}_{h_t,h_x}(t_l,\, \cdot),\, y_{h_t}(t_l)\right) = \left(\boldsymbol{u}^l_{h_x}(\cdot),\, y^l\right)$$

and

$$\left(\boldsymbol{u}_{h_t,h_x}(t_{l+1},\, \cdot),\, y_{h_t}(t_{l+1})\right) = \left(\boldsymbol{u}^{l+1}_{h_x}(\cdot),\, y^{l+1}\right)$$

We also use a piecewise constant interpolant $(\boldsymbol{v}_{h_t,h_x},\, z_{h_t})$ such that

$$\left(\boldsymbol{v}_{h_t,h_x}(t_l,\, \cdot),\, z_{h_t}(t_l)\right) = \left(\boldsymbol{v}^l_{h_x}(\cdot),\, z^l\right) \quad \text{for all } t \in (t_{l-1},\, t_l].$$

The time discrete total forces are defined by

$$N_{h_t}(t) = h_t \sum_{j=0}^{\lfloor T/h_t \rfloor - 1} \delta(t - t_{j+1})\, N^j.$$

Recall all the conditions (22–27) in the continuous case. Assume that $f_b = \sum_{j=1}^{P_s} c_j \psi_j(x)$ and $f_s = c$. In the time discretization, the implicit Euler method and the midpoint rule are applied to set up the following numerical formulations:

$$\begin{aligned} &\frac{1}{h_t}\left(\boldsymbol{v}^{l+1}_{h_x} - \boldsymbol{v}^l_{h_x}, \boldsymbol{w}_{h_x}\right) = -\frac{\alpha_b}{2} a\left(\boldsymbol{v}^{l+1}_{h_x} + \boldsymbol{v}^l_{h_x}, \boldsymbol{w}_{h_x}\right) \\ &\quad - \frac{1}{2} a\left(\boldsymbol{u}^{l+1}_{h_x} + \boldsymbol{u}^l_{h_x}, \boldsymbol{w}_{h_x}\right) + \frac{\lambda_{nc}}{2}\left(\left(\Psi - u^{l+1}_{h_x}(1)\right)^p_+ + \left(\Psi - u^l_{h_x}(1)\right)^p_+\right) w_{h_x}(1) \\ &\quad + \int_0^1 f_b w_{h_x} dx \quad \text{for all } \boldsymbol{w}_{h_x} = (\vartheta_{h_x},\, w_{h_x})^T \in V_{h_x} \end{aligned} \tag{52}$$

and

$$\frac{z^{l+1}-z^l}{h_t} = -\frac{\alpha_s}{2}\left(z^{l+1}+z^l\right) - \frac{k_1}{2}\left(y^{l+1}+y^l\right) - k_2\frac{\left(y^{l+1}\right)^2+\left(y^l\right)^2}{2}\frac{\left(y^{l+1}\right)+\left(y^l\right)}{2}$$
$$- \frac{\lambda_{nc}}{2}\left(\left(\Psi-y^{l+1}\right)_+^p + \left(\Psi-y^l\right)_+^p\right) + f_s + N^l \tag{53}$$

and

$$\frac{1}{2}\left(\boldsymbol{v}_{h_x}^{l+1}(x)+\boldsymbol{v}_{h_x}^{l}(x)\right) = \frac{1}{h_t}\left(\boldsymbol{u}_{h_x}^{l+1}(x)-\boldsymbol{u}_{h_x}^{l}(x)\right), \quad \frac{1}{2}\left(z^{l+1}+z^l\right) = \frac{1}{h_t}\left(y^{l+1}-y^l\right), \tag{54}$$

$$u_{h_x}^l(1) = y^l \quad \text{if } \varphi \le u_{h_x}^l(1) \le \Psi, \tag{55}$$

$$0 \le N^l \quad \perp \quad y^{l+1}-\varphi \ge 0, \tag{56}$$

altogether with the initial data (26–28). Note that we used the following inner product on the space H and bilinear form

$$\left(\boldsymbol{v}_{h_x}, \boldsymbol{w}_{h_x}\right)_H = \int_0^1 \omega_{h_x}\vartheta_{h_x} + v_{h_x}w_{h_x}dx \text{ and} \tag{57}$$

$$a\left(\boldsymbol{u}_{h_x}, \boldsymbol{w}_{h_x}\right) = \int_0^1 \theta'_{h_x}\vartheta'_{h_x} + \left(u'_{h_x}-\theta_{h_x}\right)\left(w'_{h_x}-\vartheta_{h_x}\right)dx, \tag{58}$$

where the primes ($'$) are the derivatives with respect to x.

Now, we define the mass matrix $\boldsymbol{M} \in \mathbb{R}^{P_s\times P_s}$, the stiffness matrix $\boldsymbol{K} \in \mathbb{R}^{P_s\times P_s}$, semi–stiffness matrix $\boldsymbol{S} \in \mathbb{R}^{P_s\times P_s}$ to be

$$\boldsymbol{M} = [m_{ij}] = \int_0^1 \psi_i(x)\psi_j(x)\,dx, \quad \boldsymbol{K} = [k_{ij}] = \int_0^1 \psi_i'(x)\psi_j'(x)\,dx,$$
$$\boldsymbol{S} = [s_{ij}] = \int_0^1 \psi_i(x)\psi_j'(x)\,dx. \tag{59}$$

In order to establish one time step nonlinear system for the Timoshenko beam equation with the normal compliance condition, we use (52) and (54) to present the following two weak formulations: find $\left(\theta_{h_x}^{l+1},\, u_{h_x}^{l+1}\right) \in V_{h_x}$ such that

$$\int_0^1 \left(\frac{2}{h_t^2}\theta_{h_x}^{l+1} - \frac{2}{h_t^2}\theta_{h_x}^{l} - \frac{2}{h_t}\omega_{h_x}^{l}\right)\vartheta_{h_x}dx = -\frac{1}{2}\int_0^1 \left(\left(\theta_{h_x}^{l+1}\right)' + \left(\theta_{h_x}^{l}\right)'\right)\vartheta'_{h_x}dx$$
$$- \frac{\alpha_b}{h_t}\int_0^1 \left(\left(\theta_{h_x}^{l+1}\right)' - \left(\theta_{h_x}^{l}\right)'\right)\vartheta'_{h_x}dx + \frac{1}{2}\int_0^1 \left(\left(u_{h_x}^{l+1}\right)' + \left(u_{h_x}^{l}\right)'\right)\vartheta_{h_x}dx$$
$$- \frac{1}{2}\int_0^1 \left(\left(\theta_{h_x}^{l+1}\right) + \left(\theta_{h_x}^{l}\right)\right)\vartheta_{h_x}dx + \frac{\alpha_b}{h_t}\int_0^1 \left(\left(u_{h_x}^{l+1}\right)' - \left(u_{h_x}^{l}\right)'\right)\vartheta_{h_x}dx$$
$$- \frac{\alpha_b}{h_t}\int_0^1 \left(\left(\theta_{h_x}^{l+1}\right) - \left(\theta_{h_x}^{l}\right)\right)\vartheta_{h_x}dx \tag{60}$$

and

$$\begin{aligned}\int_0^1 \left(\frac{2}{h_t^2}u_{h_x}^{l+1} - \frac{2}{h_t^2}u_{h_x}^{l} - \frac{2}{h_t}v_{h_x}^{l}\right) w_{h_x} dx &= -\frac{1}{2}\int_0^1 \left(\left(u_{h_x}^{l+1}\right)' + \left(u_{h_x}^{l}\right)'\right) w_{h_x}' dx \\ &+ \frac{1}{2}\int_0^1 \left(\left(\theta_{h_x}^{l+1}\right) + \left(\theta_{h_x}^{l}\right)\right) w_{h_x}' dx - \frac{\alpha_b}{h_t}\int_0^1 \left(\left(u_{h_x}^{l+1}\right)' - \left(u_{h_x}^{l}\right)'\right) w_{h_x}' dx \\ &+ \frac{\alpha_b}{h_t}\int_0^1 \left(\left(\theta_{h_x}^{l+1}\right) - \left(\theta_{h_x}^{l}\right)\right) w_{h_x}' dx + \int_0^l f_b w_{h_x} dx \\ &+ \frac{\lambda_{nc}}{2}\left(\left(\Psi - u_{h_x}^{l+1}(1)\right)_+^p + \left(\Psi - u_{h_x}^{l}(1)\right)_+^p\right) w_{h_x}(1) \end{aligned} \tag{61}$$

for all $(\vartheta_{h_x},\, w_{h_x}) \in V_{h_x}$, provided that $\left(\theta_{h_x}^l,\, u_{h_x}^l\right) \in V_{h_x}$ and $\left(\omega_{h_x}^l, v_{h_x}^l\right) \in H$ are given. From the FEM system (60–61) we solve for $\left(\theta_{h_x}^{l+1},\, u_{h_x}^{l+1}\right)$. Then a recursive relation can be written in the following block matrix form:

$$\boldsymbol{A}\begin{bmatrix} \widetilde{\theta}^{l+1} \\ \widetilde{u}^{l+1} \end{bmatrix} - h_t^2 \begin{bmatrix} \mathbf{0} \\ \widetilde{e}^{l+1} \end{bmatrix} = \boldsymbol{B}\begin{bmatrix} \widetilde{\theta}^{l} \\ \widetilde{u}^{l} \end{bmatrix} + 4h_t \begin{bmatrix} \boldsymbol{M}\widetilde{\omega}^{l} \\ \boldsymbol{M}\widetilde{v}^{l} \end{bmatrix} + 2h_t^2 \begin{bmatrix} \mathbf{0} \\ \boldsymbol{M}\widetilde{f}_b \end{bmatrix} + h_t^2 \begin{bmatrix} \mathbf{0} \\ \widetilde{e}^{l} \end{bmatrix}, \tag{62}$$

where

$$\boldsymbol{A} = \begin{bmatrix} \left(4 + h_t^2 + 2\alpha_b h_t\right)\boldsymbol{M} + \left(h_t^2 + 2\alpha_b h_t\right)\boldsymbol{K} & -\left(h_t^2 + 2\alpha_b h_t\right)\boldsymbol{S} \\ -\left(h_t^2 + 2\alpha_b h_t\right)\boldsymbol{S}^T & 4\boldsymbol{M} + \left(h_t^2 + 2\alpha_b h_t\right)\boldsymbol{K} \end{bmatrix}$$

and

$$\boldsymbol{B} = \begin{bmatrix} \left(4 - h_t^2 + 2\alpha_b h_t\right)\boldsymbol{M} + \left(2\alpha_b h_t - h_t^2\right)\boldsymbol{K} & \left(h_t^2 - 2\alpha_b h_t\right)\boldsymbol{S} \\ \left(h_t^2 - 2\alpha_b h_t\right)\boldsymbol{S}^T & 4\boldsymbol{M} + \left(2\alpha_b h_t - h_t^2\right)\boldsymbol{K} \end{bmatrix}$$

and $\widetilde{e}^l = \left(0, 0, \cdots, 0, \lambda_{nc}\left(\Psi - u_{P_s}^l\right)_+^p\right)^T \in \mathbb{R}^{P_s}$.

In order to implement the fully discrete numerical schemes, we present the pseudocode in Algorithm 1 to simulate the motion of a spring–beam system. See (1)–(4) in the Algorithm. In our simulations, a beam moves down initially. Note that $t_c = l_c h_t$ is an initial time step when the end of a beam and the top of a spring touch each other. Indeed, we pay a special attention to (5)–(28). See (11)–(13). The transmission condition is not applied to the next step solutions $\left(u_{P_s}^{l+1},\, y^{l+1}\right)$. Moreover, there are gaps between them and thus $\lambda_{nc} = 0$. See (14)–(28). The transmission condition and CCs are required to compute $\left(u_{P_s}^{l+1},\, y^{l+1}\right)$. Particularly, it is not possible to have the condition that $u_{P_S}^{l+1} < y^{l+1}$ from a physical point of view but it may happen computationally. In that case, the top of a spring and the tip of a beam are assumed to coalesce and move together. Therefore, u_{Ps}^{l+1} is temporarily assigned to the previous numerical step solution y^l. We utilize Newton–Raphson method to compute y^{l+1} at first and then u_{Ps}^{l+1} and y^{l+1} are assumed to have an identical position, as seen in (18). See (13) and (19). Since u_{Ps}^{l+1} is found in the previous steps and the matrix $\boldsymbol{A}$ in the recursive relation (62) can be partitioned into appropriate submatrices, the back–substitution allows us to compute $\left(\widetilde{\theta}^{l+1},\, \left(u_1^{l+1},\, u_2^{l+1},\, \cdots u_{P_s-1}^{l+1}\right)^T\right)$. Once the next step approximations $\left(\widetilde{\theta}^{l+1},\, \widetilde{u}^{l+1},\, y^{l+1}\right)$ are computed, (54) can be used to update $\left(\widetilde{\omega}^{l+1},\, \widetilde{v}^{l+1},\, z^{l+1}\right)$.

In the fully discrete case, the energy function at each time step $t = t_l$ is defined by

$$E_D\left(t_l\right) := E_D^l = E_{b,D}^l + E_{s,D}^l, \tag{63}$$

where

$$E_{b,D}^{l} := E_{b,D}\left(t_l\right) = \frac{1}{2}\left(\widetilde{\omega}^{l}\boldsymbol{M}\left(\widetilde{\omega}^{l}\right)^{T} + \widetilde{v}^{l}\boldsymbol{M}\left(\widetilde{v}^{l}\right)^{T}\right)$$

(64)

$$+\frac{1}{2}\left(\widetilde{\theta}^{l}\boldsymbol{K}\left(\widetilde{\theta}^{l}\right)^{T} + \widetilde{u}^{l}\boldsymbol{K}\left(\widetilde{u}^{l}\right)^{T} - 2\widetilde{u}^{l}\boldsymbol{S}^{T}\left(\widetilde{\theta}^{l}\right)^{T} + \widetilde{\theta}^{l}\boldsymbol{M}\left(\widetilde{\theta}^{l}\right)^{T}\right) - \widetilde{f}_{b}\boldsymbol{M}\left(\widetilde{u}^{l}\right)^{T},$$

(65)

$$E_{s,D}^{l} := E_{s,D}\left(t_l\right) = \frac{1}{2}\left(\left(z^{l}\right)^{2} + k_1\left(y^{l}\right)^{2} + \frac{k_2}{2}\left(y^{l}\right)^{4}\right) - c\,y^{l}.$$

where $\widetilde{f}_b = (c_1, c_2, \cdots, c_{P_s})$.

In the following Lemma 7, we will see that the total energy for this mechanical system is bounded, which may validate numerical stability of the algorithms.

Lemma 7. *Let α_b, $\alpha_s \geq 0$. Assume that the fully discrete numerical solutions $(\boldsymbol{u}_{h_t,h_x}, \boldsymbol{v}_{h_t,h_x}, y_{h_t}, z_{h_t})$ satisfy (52–56). Then $E_D^l \leq M < \infty$ for any $l \geq 0$ with h_t, $h_x > 0$.*

Proof. Take $\boldsymbol{w}_{h_x} = \frac{1}{2}\left(\boldsymbol{v}^{l+1}(x) + \boldsymbol{v}^{l}(x)\right) \in V_{h_x}$ and $\boldsymbol{w}_{h_x} = \frac{1}{h_t}\left(\boldsymbol{u}^{l+1}(x) - \boldsymbol{u}^{l}(x)\right) \in V_{h_x}$ in the first one of (54). Then it is easy to see from (52) that for $h_t > 0$

$$\begin{aligned}
&\frac{1}{2h_t}\left(\left(\boldsymbol{v}_{h_x}^{l+1}, \boldsymbol{v}_{h_x}^{l+1}\right) - \left(\boldsymbol{v}_{h_x}^{l}, \boldsymbol{v}_{h_x}^{l}\right)\right) + \frac{\alpha_b}{2}a\left(\boldsymbol{v}_{h_x}^{l+1} + \boldsymbol{v}_{h_x}^{l}, \boldsymbol{v}_{h_x}^{l+1} + \boldsymbol{v}_{h_x}^{l}\right) \\
&\quad + \frac{1}{2h_t}\left(a\left(\boldsymbol{u}_{h_x}^{l+1}, \boldsymbol{u}_{h_x}^{l+1}\right) - a\left(\boldsymbol{u}_{h_x}^{l}, \boldsymbol{u}_{h_x}^{l}\right)\right) - \frac{1}{h_t}\int_0^1 f_b\left(u_{h_x}^{l+1} - u_{h_x}^{l}\right)dx \\
&\quad = \frac{\lambda_{nc}}{2h_t}\left(\left(\Psi - u_{P_s}^{l+1}\right)_+^{p} + \left(\Psi - u_{P_s}^{l}\right)_+^{p}\right)\left(u_{P_s}^{l+1} - u_{P_s}^{l}\right).
\end{aligned} \tag{66}$$

It follows from (57–58) and (59) that for each time step $t = t_l$

$$\left(\boldsymbol{v}_{h_x}^{l}, \boldsymbol{v}_{h_x}^{l}\right) = \widetilde{\omega}^{l}\boldsymbol{M}\left(\widetilde{\omega}^{l}\right)^{T} + \widetilde{v}^{l}\boldsymbol{M}\left(\widetilde{v}^{l}\right)^{T}, \tag{67}$$

$$a\left(\boldsymbol{u}_{h_x}^{l}, \boldsymbol{u}_{h_x}^{l}\right) = \widetilde{\theta}^{l}\boldsymbol{K}\left(\widetilde{\theta}^{l}\right)^{T} + \widetilde{u}^{l}\boldsymbol{K}\left(\widetilde{u}^{l}\right)^{T} - 2\widetilde{u}^{l}\boldsymbol{S}\left(\widetilde{\theta}^{l}\right)^{T} + \widetilde{\theta}^{l}\boldsymbol{M}\left(\widetilde{\theta}^{l}\right)^{T}, \text{ and} \tag{68}$$

$$\int_0^1 f_b\boldsymbol{u}_{h_x}^{l}dx = \widetilde{f}_b\boldsymbol{M}\left(\widetilde{u}^{l}\right)^{T}. \tag{69}$$

One can notice that $\widetilde{u}^{l}\boldsymbol{S}^{T}\left(\widetilde{\theta}^{l}\right)^{T} = \widetilde{\theta}^{l}\boldsymbol{S}\left(\widetilde{u}^{l}\right)^{T}$. We plug (67–69) into the equation (66). Then we can obtain

$$E_{b,D}^{l+1} \leq E_{b,D}^{l} + \lambda_{nc}\left(\left(\Psi - u_{P_s}^{l+1}\right)_+^{p} + \left(\Psi - u_{P_s}^{l}\right)_+^{p}\right)\left(u_{P_s}^{l+1} - u_{P_s}^{l}\right). \tag{70}$$

Since numerical solutions $u_{h_t,h_x}(t,\cdot)$ are piecewise linear continuous on $[0, T]$, it follows from (55–56) that

$$E_{b,D}^{l+1} \leq E_{b,D}^{l} + 2\lambda_{nc}\left(\Psi - \varphi\right)^{p} O\left(h_t\right), \tag{71}$$

Algorithm 1 Computation for fully discrete numerical solutions

Initial data: $\widetilde{\theta}^0$, $\widetilde{u}^0$, $\widetilde{\omega}^0$, and $\widetilde{v}^0 \in \mathbb{R}^{P_s}$ are given

(1) for $i = 1 : l_c - 1$
(2) $\quad \lambda_{nc} \leftarrow 0$;
(3) $\quad$ update $\widetilde{\theta}^{l+1}$, $\widetilde{u}^{l+1}$, $\widetilde{\omega}^{l+1}$, $\widetilde{v}^{l+1}$ from the previous data $\widetilde{\theta}^l$, $\widetilde{u}^l$, $\widetilde{\omega}^l$, $\widetilde{v}^l$;
(4) end for % there is no contact until the end of beam touches the top of a spring.
(5) $y^{l_c} \leftarrow \Psi$ and $z^{l_c} \leftarrow v^{l_c}_{P_s}$;
(6) $\lambda_{nc} > 0$ is chosen; % there is an initial contact between them.
(7) for $l = l_c : \lfloor T/h_t \rfloor - 1$
(8) $\quad$ the previous data are given by $\widetilde{\theta}^l$, $\widetilde{u}^l$, $\widetilde{\omega}^l$, $\widetilde{v}^l \in \mathbb{R}^{P_s}$ and y^l, $z^l \in \mathbb{R}$;
(9) $\quad$ compute $\widetilde{u}^{l+1}$ from the iterative formula (62);
(10) $\quad$ compute $\left(y^{l+1}, z^{l+1}\right)$ from (53–54);
(11) $\quad$ if $y^{l+1} > \Psi$ and $y^{l+1} < u^{l+1}_{P_s}$
(12) $\quad\quad \lambda_{nc} \leftarrow 0$; % There is no contact between them.
(13) $\quad\quad$ compute $\left(\widetilde{\theta}^{l+1}, \left(u^{l+1}_1, u^{l+1}_2, \cdots u^{l+1}_{P_s-1}\right)^T\right)$ from (62);
(14) $\quad$ elseif $u^{l+1}_{P_s} \le \Psi$ or $u^{l+1}_{P_s} \le y^{l+1}$
(15) $\quad\quad \lambda_{nc} > 0$ is chosen; % it will be the same value as in (6).
(16) $\quad\quad y^l_{temp} \leftarrow u^{l+1}_{P_s}$; % accommodate the transmission condition.
(17) $\quad\quad$ compute $\left(y^{l+1}, z^{l+1}\right)$ from (53–54);
(18) $\quad\quad u^{l+1}_{P_s} \leftarrow y^{l+1}$;
(19) $\quad\quad$ compute $\left(\widetilde{\theta}^{l+1}, \left(u^{l+1}_1, u^{l+1}_2, \cdots u^{l+1}_{P_s-1}\right)^T\right)$ from (62);
(20) $\quad\quad$ if $y^{l+1} == \varphi$ % compute the next step numerical solutions satisfying CCs.
(21) $\quad\quad\quad u^{l+1}_{P_s} \leftarrow \varphi$;
(22) $\quad\quad\quad$ compute $\left(\widetilde{\theta}^{l+1}, \left(u^{l+1}_1, u^{l+1}_2, \cdots u^{l+1}_{P_s-1}\right)^T\right)$ from (62);
(23) $\quad\quad\quad y^{l+1} \leftarrow \varphi$;
(24) $\quad\quad\quad$ compute N^l from (53); compute z^{l+1} from (54);
(25) $\quad\quad$ else if $y^{l+1} > \varphi$
(26) $\quad\quad\quad N^l \leftarrow 0$;
(27) $\quad\quad$ end if
(28) $\quad$ end if
(29) $\quad$ use (54) to compute $\left(\widetilde{\omega}^{l+1}, \widetilde{v}^{l+1}, z^{l+1}\right)$;
(30) $\quad \widetilde{\theta}^l \leftarrow \widetilde{\theta}^{l+1}$; $\widetilde{u}^l \leftarrow \widetilde{u}^{l+1}$; $\widetilde{\omega}^l \leftarrow \widetilde{\omega}^{l+1}$; $\widetilde{v}^l \leftarrow \widetilde{v}^{l+1}$; $y^l \leftarrow y^{l+1}$; $z^l \leftarrow z^{l+1}$;
(31) end for

where the big O notation is used. Similarly, it follows from (53) and the second one in (54) that

$$\begin{aligned}
&\frac{1}{2h_t}\left(\left(z^{l+1}\right)^2 - \left(z^l\right)^2\right) + \frac{\alpha_s}{4}\left(z^{l+1} + z^l\right)^2 + \frac{k_1}{2}\left(\left(y^{l+1}\right)^2 - \left(y^l\right)^2\right) \\
&\quad + \frac{k_2}{4}\left(\left(y^{l+1}\right)^4 - \left(y^l\right)^4\right) - \frac{1}{h_t}N^l\left(y^{l+1} - \varphi\right) + \frac{1}{h_t}N^l\left(y^l - \varphi\right) - \frac{c}{h_t}\left(y^{l+1} - y^l\right) \\
&\quad = -\frac{\lambda_{nc}}{2h_t}\left(\left(\Psi - y^{l+1}\right)_+ + \left(\Psi - y^l\right)_+\right)\left(y^{l+1} - y^l\right).
\end{aligned} \tag{72}$$

TABLE 1. Selected fixed data.

κ_1	κ_2	α_b	α_s	f_s	λ_{nc}	p	Ψ	φ	T
3.6×10^{10}	3.6×10^{10}	0	0	0	10^4	3	0	-0.015	4

The CCs in (56) gives the following inequality:

$$E_{s,D}^{l+1} \leq E_{s,D}^{l} - \frac{\lambda_{nc}}{2h_t}\left(\left(\Psi - y^{l+1}\right)_+ + \left(\Psi - y^{l}\right)_+\right)\left(y^{l+1} - y^{l}\right). \tag{73}$$

Since numerical solutions y_{h_t} are also piecewise linear continuous on $[0,\, T]$, we can easily see that

$$E_{s,D}^{l+1} \leq E_{s,D}^{l} + 2\lambda_{nc}\left(\Psi - \varphi\right)^p O\left(h_t\right). \tag{74}$$

Thus a telescoping sum allows us to have

$$E_D^l \leq E^0 + Clh_t \leq E^0 + CT = M < \infty,$$

as desired. □

Note that if the top of springs and the end of beams are not separate, then energy does not increase which can be easily proved.

6. Numerical results and discussion

In this section, we implement the numerical schemes proposed in the previous section 5. We reduce the number of all the coefficients in the Timoshenko beam equations (1–2) and modify the extended Duffing equation (6) to present the following simplified forms:

$$\begin{aligned}
&\theta_{tt} = \kappa_1\theta_{xx} + \kappa_2\left(u_x - \theta\right) + \alpha_b\,\kappa_1\theta_{txx} + \alpha_b\,\kappa_2\left(u_{tx} - \theta_t\right),\\
&u_{tt} = \kappa_2\left(u_{xx} - \theta_x\right) + \alpha_b\,\kappa_2\left(u_{txx} - \theta_{tx}\right) + f_b,\\
&y_{tt} + \alpha_s y_t + k_1\, y + k_2 y^3 = -\lambda_{nc}\left(\Psi - u(t,\,1)\right)_+^p + N(t) + f_s.
\end{aligned}$$

The initial data to be chosen are presented as follows:

$$\theta^0(x) = 0,\ \theta_t^0(x) = 0,\ u^0(x) = 0.5x,\ u_t^0(x) = -x,\ y\left(t_c\right) = \Psi,\ y_t\left(t_c\right) = 0,\ N(0) = 0,$$

where $t_c \in (0,\, T]$ is an initial contact time. Note that the boundary conditions (4–5) can also be easily adjusted. All the selected data are presented in the Table 1.

In our numerical experiments, we assume that $u_t\left(t_c^-,\,1\right) = u_t\left(t_c^+,\,1\right)$. As seen in the Table, a spring–beam system consists of a purely elastic Timoshenko beam and nonlinear spring. We will also choose different coefficients k_1, k_2 for a nonlinear spring to make observations on their different motion. The time step size and the size of subintervals are $h_t = 0.004$ and $h_x = 0.001$, respectively. Therefore, the size of the block matrices $\boldsymbol{A}$, $\boldsymbol{B}$ in (62) is $2,000 \times 2,000$. Matlab's sparse matrix utility enables for us to provide an efficient computation for the iterative formula (62).

This physical setting is quite similar to one considered in [10] but in the paper the beams touch a rigid foundation, instead of a deformable foundation. There are two groups to display our numerical simulations. We use the different quantities $k_1 > 0$ and $k_2 < 0$ for each group. We note that in the Duffing equation, quantities k_2 can be negative but have to be close to zero. The beams are assumed to move downward initially and be undeformed until their right end touches the top of the spring. All the projected curves in sub-figure (A) of Figures 2–5 are captured at each time step, right after the tip of the beams hits the top of the spring. Subsequently, the curves

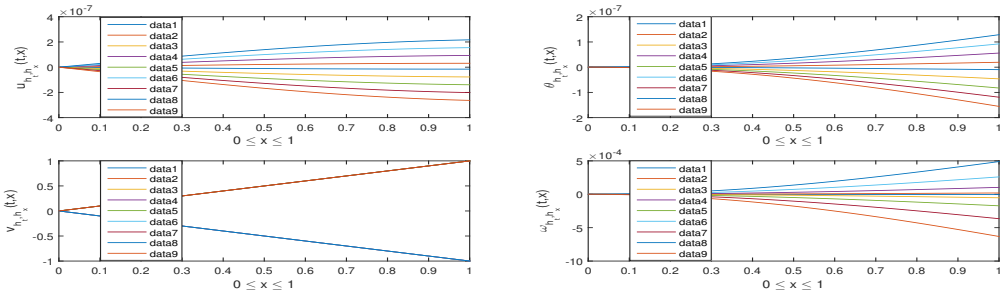

(A) Motion of the beam right after contact

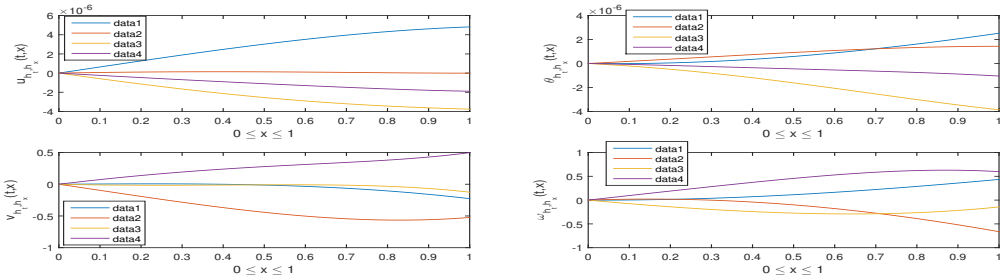

(B) Subsequent motion of the beam

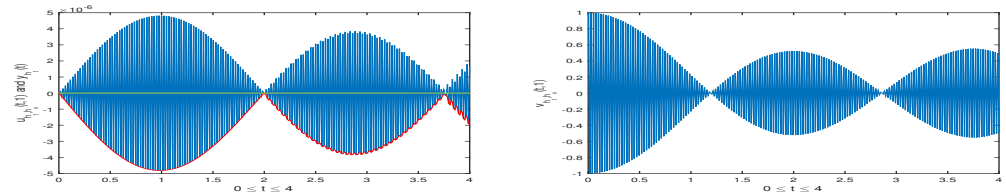

(C) Position of the beam's tip and top of the spring and velocity of the beam's tip

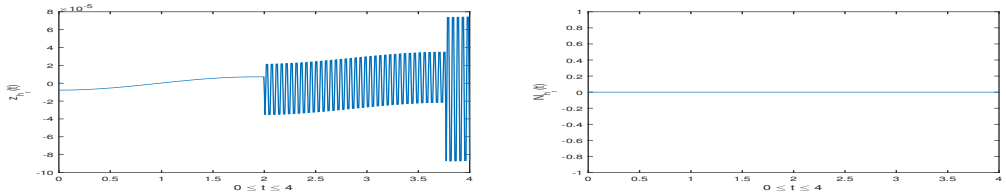

(D) Velocity of top of the spring and magnitude of contact forces

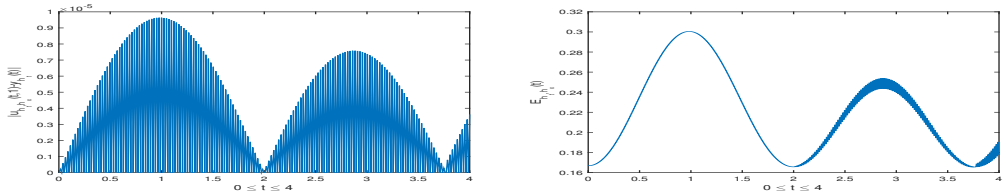

(E) Gap and the total energy

FIGURE 2. $k_1 = 3$, $k_2 = -0.2$, $f_b = \mathbf{0}$.

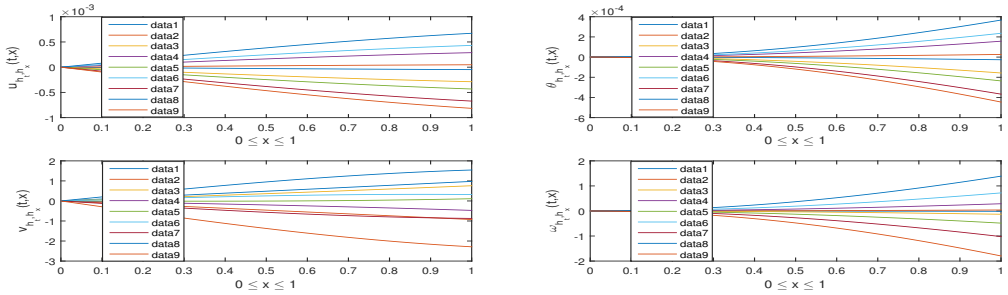

(A) Motion of the beam right after contact

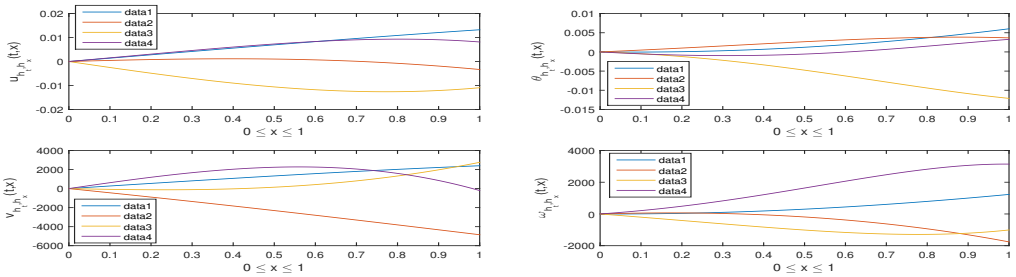

(B) Subsequent motion of the beam

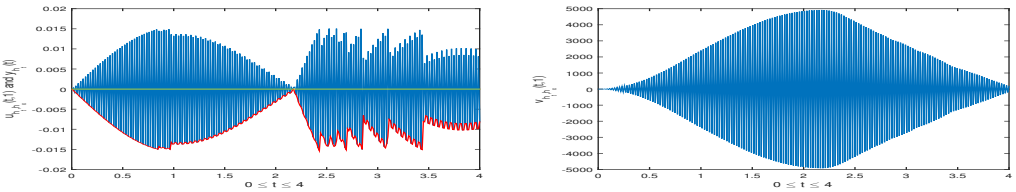

(C) Position of the beam's tip and top of the spring and velocity of the beam's tip

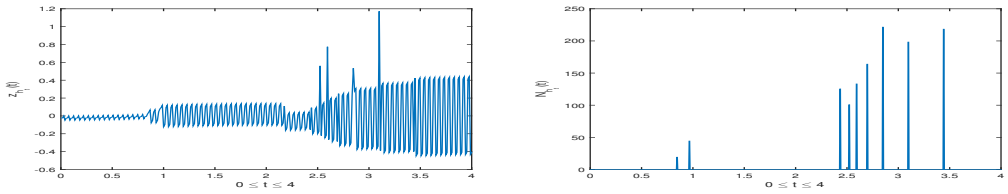

(D) Velocity of top of the spring and magnitude of contact forces

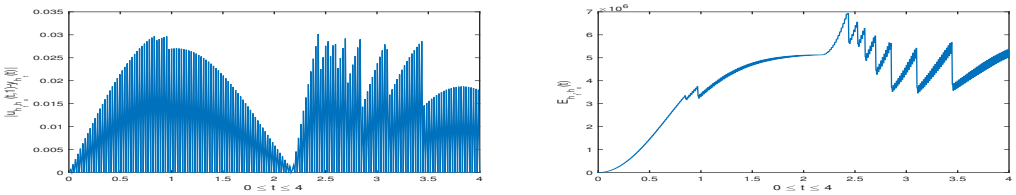

(E) Gap and the total energy

FIGURE 3. $k_1 = 3$, $k_2 = -0.2$, $f_b = (0, 0, \cdots, -6)$.

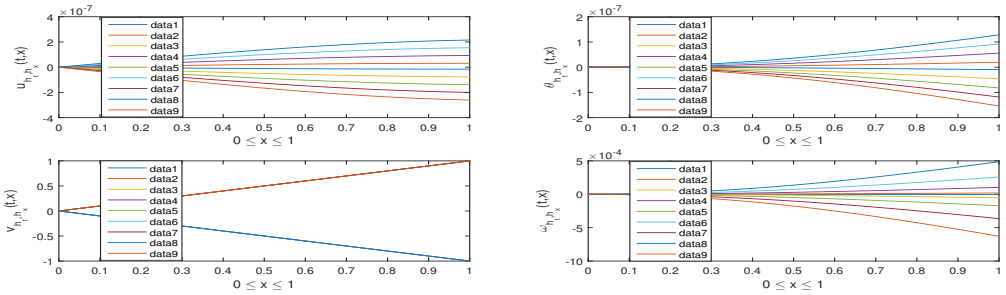

(A) Motion of the beam right after contact

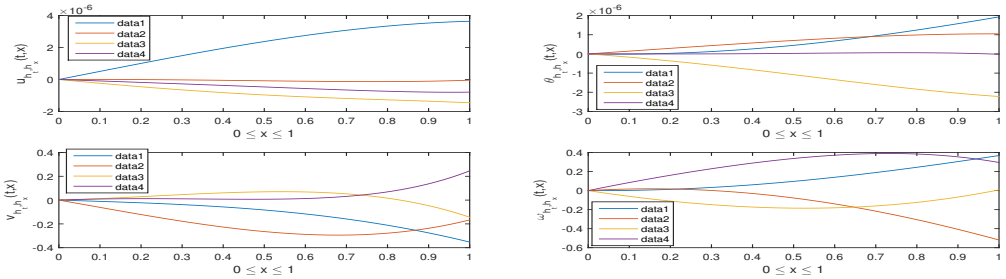

(B) Subsequent motion of the beam

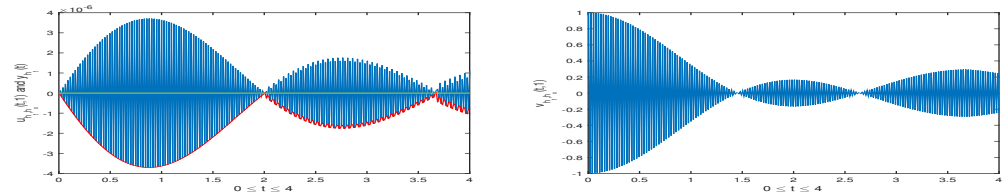

(C) Position of the beam's tip and top of the spring and velocity of the beam's tip

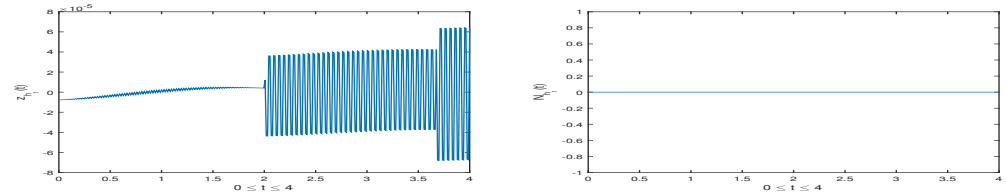

(D) Velocity of top of the spring and magnitude of contact forces

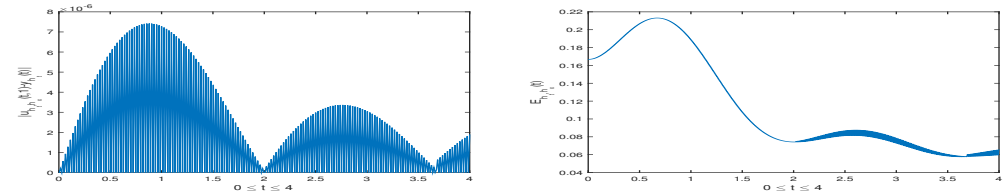

(E) Gap and the total energy

FIGURE 4. $k_1 = 150$, $k_2 = 67$, $f_b = \mathbf{0}$.

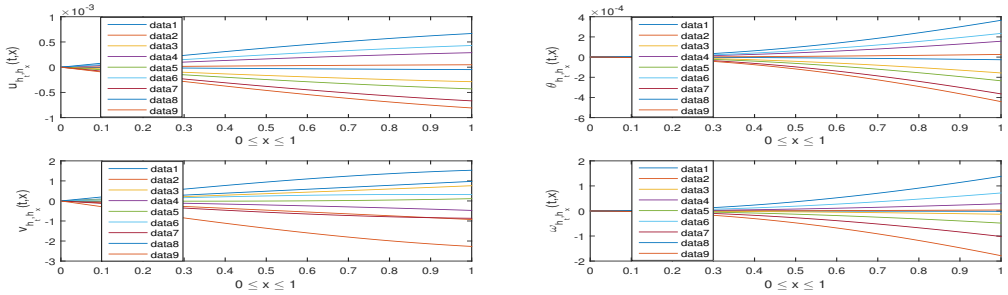

(A) Motion of the beam right after contact

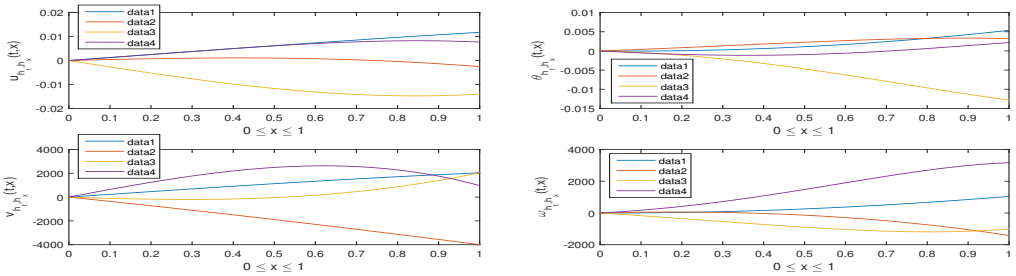

(B) Subsequent motion of the beam

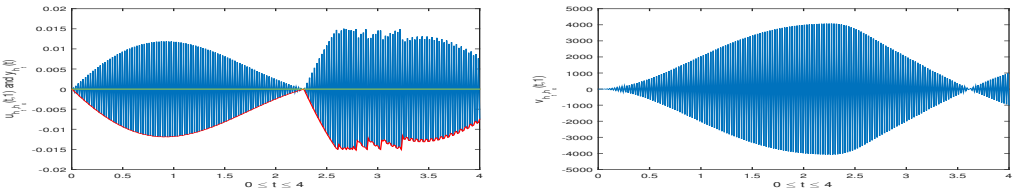

(C) Position of the beam's tip and top of the spring and velocity of the beam's tip

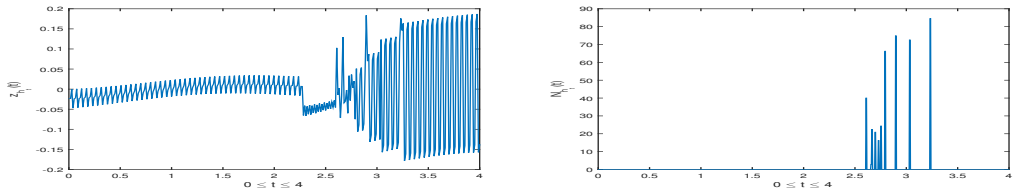

(D) Velocity of top of the spring and magnitude of contact forces

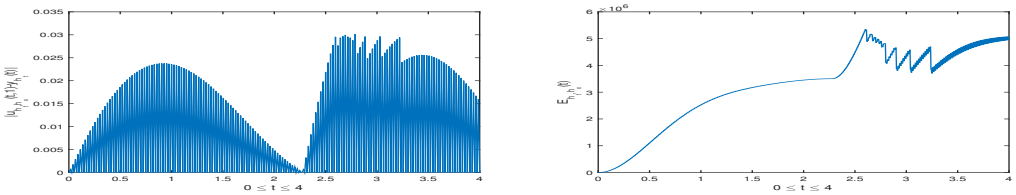

(E) Gap and the total energy

FIGURE 5. $k_1 = 150$, $k_2 = 67$, $f_b = (0, 0, \cdots, -6)$.

TABLE 2. Computing each time step numerical solutions.

	Figure 2	Figure 3	Figure 5	Figure 5
Average # of Newton's iterations	1.990	3.0100	2.0000	2.9780
Average elapsed time (sec)	5.63×10^{-3}	5.84×10^{-3}	5.90×10^{-3}	5.83×10^{-3}

in sub–figures (B) are sampled at every 249 time step. One can refer to the boxes in each picture to see how the beams oscillate. Particularly, see the left bottom pictures about $v_{h_t,h_x}(t,x)$ in sub-figure (A) of Figures 2 and 4. One can observe that the beams move up and down almost the same speed at each time step.

See sub-figures (C)–(E) in each of Figures. While the magnitude of contact forces and the total energy are sampled every time step in (E), all the numerical solutions are sampled every third time step in sub-figures (C) and (D) to avoid possibilities of higher frequencies. See the left pictures in sub-figure (C) of each Figure. The blue and red lines show the motion of the beam's tip and the spring's top, respectively. We can confirm the numerical evidence that the numerical solutions satisfy the transmission condition in (55). An interesting point is that the spring's top does not seem to pass the equilibrium position Ψ. However, when we zoom in the picture in sub-figure (C) of Figure 4 we can barely see that $0 = \Psi < y_{h_t}(t) < u_{h_t,h_x}(t,1)$ around $t = 3.6$. This shows a numerical evidence that solutions do not satisfy the transmission condition necessarily if the top of spring and the beam's tip are positioned higher than Ψ. A little wiggling (see the red color) is detected over some local intervals. One can guess that this is due to the beam's hitting. We also observe that they continue to touch each other and separate alternatively, which may be understood by the Newton's third law. Therefore, the numerical simulations are fairly reasonable from the physical perspective. However, there are significant oscillations of the beam's tip, due to the continued hit–separation at each time step. This implies that they may cause noisy solutions and numerical instability. Indeed, the task of computing numerical approximations for dynamic contact problems still remains elusive in contact mechanics. In the recent paper [29], the numerical schemes have been improved to avoid the unstable numerical solutions. Another interesting point (see the right picture in sub-figure (C) of Figures 2–5) is that the load f_b applied at the tip makes much faster vibrations, after the initial contact time $t = t_c$. See the pictures in sub-figure (D) of Figures 3 and 5. There are sudden big changes in the velocity of the spring at some time steps and there occurs contact forces then. Accordingly, the numerical solutions are validated to satisfy the CCs in (8) as well. We compare the left picture in sub-figure (D) of Figure 3 with one in (D) of Figure 5. The velocity of the softer spring produces sudden changes more sharply than the stiffer one does. Consequently, the softer one causes higher singular contact forces than the stiffer one does. As we proved the boundedness of the total energy in Lemma 7, it is reasonably supported by the numerical evidence displayed in sub-figure (D) of all Figures.

The following Table 2 displays our numerical computation performance. When y_{h_t} is computed at each time step, the tolerance $\epsilon = 10^{-12}$ in Newton–Raphson method is taken through all the numerical experiments. We note that the semi-smooth function $(\cdot)_+$ can be a smooth function, if $p > 1$.

7. Acknowledgments

The authors would like to thank the referees for their valuable comments, which have improved the presentation of the paper.

References

[1] J. J. Moreau and P. D. Panagiotopoulos and G. Strang, Topics in Nonsmooth Mechanics, Birkhäuser Verlag, Basel, Boston, Berlin, 1988.

[2] Emily Winkler, Die Lehre von der Elasticitaet und Festigkeit mit besondere Ruecksicht auf ihre Anwendung in der Technik, fuer polytechnische Schuhlen, Bauakademien, Ingenieure, Maschienenbauer, Architecten, etc. Vortraege ueber Eisenbahnba, Vol. 1, Prague: H. Dominicus, 1867.

[3] Michael J Brennan and Ivana Kovavic, The Duffing equation: Nonlinear oscillators and their behaviour, Wiley. Hoboken, NJ, USA, 2011.

[4] Earl A. Coddington and Norman Levinson, Theory of Ordinary Differential Equations, Originally publishedl 1955, New York, MacGraw Hill, 1984.

[5] H. Triebel, Interpolations Theory, Function Spaces, Differential Operators, North Holland, Amsterdam, 1978.

[6] Meir Shillor and Mircea Sofonea and Jożef Joachim. Telega, Models and Analysis of Quasistatic Contact, Lecture Notes in Physics, Springer, Berlin, 2004.

[7] Mircea Sofonea and Weimin Han and Meri Shillor, Analysis and Approximation of Contact problems with Adhesion and Damage, hapman & Hall/CRC, Boca Raton, FL, USA, 2006.

[8] Jeongho Ahn, The generalized Duffing equation with temperature-dependent friction, in progress.

[9] Christine Bernardi and Maria Inês M. Copetti, Discretization of a nonlinear dynamic thermoviscoelastic Timoshenko beam model, ZAMM, 97, 5, 2017, 532-549.

[10] Jeongho Ahn and David E. Stewart, A viscoelastic Timoshenko beam with dynamic frictionless impact, Discrete and continuous dynamical system series B, 12, 1, 2009, 1-22.

[11] Stephen Timoshenko, On the correction for shear of the differential eqution fortransverse vibrations of prismatic bars, Philoshophical Magazine, 41, 1921, 744-766.

[12] Stephen Timoshenko, On the transverse vibrations of bars of uniform cross-section, Philosophical Magazine, 43, 1922, 125-131.

[13] A. Klarbring and A. Mikelic and M. Shillor, Frictional contact problems with normal compliance, Int. J. Engng. Sci, 26, 8, 1988, 811-832.

[14] J. A. C Martins and J. T. Oden, A numerical analysis of a class of problems in elastodynamics with friction, Comput. Meth. Appl. Mech. Engnr, 40, 1983, 327-360.

[15] K. T. Andrews and Meir Shillor and S. Wright, On the dynamic vibration of an elastic beam in frictional contat with a rigid obdtacle, J. Elasticity, 42, 1996, 1-30.

[16] J. Bajkowski and Kenneth Kuttler and Meir Shillor, A thermoviscoelastic beam model for brakes, European Journal of Applied Mathematics, 15, 2, 2004, 181-202.

[17] R. J. Gu and Kenneth Kuttler and Meir Shillor, Frictional wear of a thermoelastic beam, Journal of mathematical analysis and applications, 242, 2000, 212-236.

[18] Kenneth Kuttler and Yves Renard and Meir Shillor, Models and simulations of dynamic frictional contact of a beam, Computer methods in applied mechanics and engineering, 177, 1999, 259-272.

[19] K. T. Andrews and M. F. M'Bengue and M. Shillor, Vibrations of a nonlinear dynamic beam between two stops, Discrete and Continuous Dynamical Systems Series B, 12, 1, 2009, 23–38.

[20] K.T. Andrews and Y. Dumont and M.F. M'Bemgue and J. Purcell and M. Shillor, Analysis and simulations of a nonlinear elastic dynamic Beam, ZAMP, 63, 2012, 1005–1019.

[21] Jeongho Ahn, Dyanmic frictional thermoviscoelastic Gao beams, ZAMP, 72, 194, 2021.

[22] Jeongho Ahn and K. L. Kuttler and M. Shillor, Modeling, analysis and simulations of a dynamic thermoviscoelastic rod-beam system, Differ Equ Dyn Syst, 25, 4, 2017, 527-552.

[23] Jeongho Ahn and David E. Stewart, An Euler-Bernoulli beam with dynamic contact:discretization, convergence, and numerical results, SIAM J. Numer. Anal., 43, 4, 2005, 1455-1480.

[24] Vasile Marinca and Nicolae Herisanu, Explicit and exact solutions to cubic Duffing and double-well Duffing equations, Mathematical and Computer Modelling, 53, 2011, 604-609.

[25] H. Askari and Z. Saadatnia and D. Younesian and A. Yildirim and M. Kaliami-Yazdi, Approximate periodic solutions for the Helmholtz-Duffing equation, Computers and Mathematics with Applications, 62, 2011, 3894-3901.

[26] Alex Elías-Zúñiga, Aalytical solutions of the damped Helmholtz-Duffing equation, Applied Mathematics Letters, 25, 2012, 2349-2353.

[27] Alex Elías-Zúñiga, Exact solution of the cubix-quintic Duffing oscillator, Applied Mathematical Modelling, 32, 2013, 2574-2579.

[28] Jeongho Ahn and Zachary Rail, A rod-beam system with dynamic contact and thermal exchange condition, Applied Mathematics and Computation, 388, 2021.
[29] Jose A. González and Ján Kopačka and Radek Kolman and Kwang-Chun Park, Partitioned formulation of contact–impact problems with stabilized contact constraints and reciprocal mass matrices, Int J Numerical Methods Eng., 122, 2021, 4609-4636.

Department of mathematics and statistics, Arkansas State University, Jonesboro, AR 72464, USA

E-mail: jahn@astate.edu and nicholas.tate@smail.astate.edu